2. EXPLANATORY NOTES[1]

Shipboard Scientific Party[2]

INTRODUCTION

In this chapter, we have assembled information that will help the reader understand the observations on which our preliminary conclusions are based and also help the interested investigator select samples for further analysis. This information concerns only shipboard operations and analyses described in the site reports in the *Initial Reports* volume of the Leg 162 *Proceedings of the Ocean Drilling Program.* Methods used by various investigators for shore-based analyses of Leg 162 data will be described in the individual scientific contributions to be published in the *Scientific Results* volume.

The separate sections of the site chapters were written by the shipboard scientific specialists for each scientific discipline (see "Participants Aboard the *JOIDES Resolution* for Leg 162" at the front of this volume).

Drilling Operations

Three coring systems were used during Leg 162: the advanced hydraulic piston corer (APC), the extended core barrel (XCB), and the rotary core barrel (RCB). Each of these systems was applied to maximize core recovery in the lithology being drilled. Drilling systems and their characteristics, such as drilling related deformation, are summarized in the "Explanatory Notes" chapters of various previous *Initial Reports* volumes. The Leg 139 *Initial Reports* volume includes a particularly detailed description.

Drilled intervals are referred to in meters below rig floor (mbrf), which is measured from the kelly bushing on the rig floor to the bottom of the drill pipe, and in meters below seafloor (mbsf), which is calculated. In the case where sediments of substantial thickness cover the seafloor (as at all sites visited during Leg 162), the "mbrf" depth of the seafloor is determined with a mudline core, assuming 100% recovery for the cored interval in the first core. Water depth is calculated by subtracting the distance from the rig floor to sea level from the mudline measurement (in mbrf). Note that this water depth usually differs from precision depth recorder (PDR) measurements by a few to several meters. The "mbsf" depths of core tops are calculated by subtracting the seafloor depth (in mbrf) from the core top depth (in mbrf). The core top datums from the driller are the ultimate depth reference for any further depth calculation procedures.

Curatorial Procedures and Sample Depth Calculations

Numbering of sites, holes, cores, and samples follows the standard ODP procedure. A full curatorial identifier for a sample consists of the following information: leg, site, hole, core number, core type, section number, and interval in centimeters measured from the top of the section. For example, a sample identification of "162-980A-10H-1, 10–12 cm" would be interpreted as representing a sample removed from the interval between 10 and 12 cm below the top of Section 1, Core 10 ("H" designates that this core was taken with the APC system) of Hole 980A at Site 980 during Leg 162.

Cored intervals are also referred to in curatorial meters below seafloor. The mbsf depth of a sample is calculated by adding the depth of the sample below the section top and the lengths of all higher sections in the core to the core top datum measured with the drill string. Note that a sediment core from less than a few hundred meters below seafloor expands upon recovery (typically 10% in upper 300 m) and its length does not match the drilled interval it originates from. In addition, there is typically a coring gap between cores, as shown by composite depth construction (see below). Thus, a discrepancy exists between the drilling mbsf and the curatorial mbsf. For instance, the curatorial mbsf of a sample taken from the bottom of a core is larger than that from a sample from the top of the subsequent core, while the latter does correspond to the drilled core top datum.

During Leg 162, multiple holes (typically three) were drilled at a site to construct a continuous composite section. This resulted in a "meters composite depth" (mcd) scale for each site, which accommodates core expansion and drilling gaps through interhole correlation using continuous measurements of core physical properties (see "Composite Depth" section, this chapter). Within the top 300 m of sediment, the "mcd" scale is typically expanded relative to the drilling mbsf scale by 10%.

Core Handling and Analysis

General core handling procedures are described in previous *Initial Reports* volumes and in the Shipboard Scientist's Handbook, and are summarized here. As soon as cores arrived on deck, gas void samples were taken by means of a vacutainer, if applicable, for immediate analysis as part of the shipboard safety and pollution prevention program. Core-catcher samples were taken for biostratigraphic analysis. When the core was cut in sections, whole-round samples were taken for shipboard interstitial water examinations. In addition, headspace gas samples were immediately scraped from the ends of cut sections and sealed in glass vials for light hydrocarbon analysis.

Before splitting, whole-round core sections were run through the multisensor track (MST) and thermal conductivity measurements were performed on sections relevant for heat-flow studies. The cores were then split into working and archive halves, from bottom to top, so investigators should be aware that older material could have been transported upward on the split face of each section. The working half of each core was sampled for both shipboard analysis, such as physical properties, carbonate and bulk X-ray diffraction mineralogy, and shore-based studies. The archive half was described visually and by means of a hand-held color scanner and smear slides. Most archive sections were run through the cryogenic magnetometer and an automated color reflectance scanning system. The archive half was then photographed with both black-and-white and color film, a whole core at a time, and close-up photographs (black-and-white) were taken of particular features for illustrations in site summaries, as requested by individual scientists.

Both halves of the core were then put into labeled plastic tubes, sealed, and transferred to cold storage space aboard the ship. At the end of the leg, the cores were transferred from the ship into refriger-

[1]Jansen, E., Raymo, M.E., Blum, P., et al., 1996. *Proc. ODP, Init. Repts.,* 162: College Station, TX (Ocean Drilling Program).

[2]Shipboard Scientific Party is given in the list preceding the Table of Contents.

ated trucks and to cold storage at the Bremen Core Repository of the Ocean Drilling Program.

UNDERWAY GEOPHYSICS AND SEISMIC STRATIGRAPHY

Instrumentation

Navigation

The Global Positioning System (GPS) was used throughout Leg 162, with a Magnavox Model MX1107 receiver placed in the underway geophysics laboratory. The receiving antenna is located 28 m forward of the stern and 46 m aft of the drill floor, but corrections were applied so that the positions recorded correspond to the drill floor location. Positions were logged once every minute during transit between sites, and every 8 seconds (equal to seismic shot intervals) during site surveys. GPS fixes were available continuously, and with the exception of occasional periods lasting no more than a few minutes, stable positioning was achieved throughout the leg. While on site, almost all GPS positions logged at 1-min intervals were within a circle of 100-m radius, which is also considered to be the accuracy of the GPS navigation.

Navigation data were logged and real-time track plots were generated by the navigation software system WINFROG, mounted on a dedicated PC in the underway geophysics laboratory. Subsequent processing and display of navigation data were performed using the Generic Mapping Tool (GMT) software package (Wessel and Smith, 1991).

Echosounders

Two low-frequency echosounders (precision depth recorders, or PDRs), running at 3.5 kHz and 12 kHz, respectively, were used to acquire bathymetric data, as well as high-resolution reflection records of the uppermost sediment layers. Data from both systems were recorded on Raytheon Model 1807M analog line-scanning recorders. Both the 3.5-kHz and the 12-kHz PDRs used a Raytheon CESP III Correlator Echo Sounder Processor driven by a Raytheon PTR 105B transceiver with a 2-kW sonar transmitter. The 3.5-kHz PDR used an array of 12 MASSA TR-1075SF transducers, while the 12-kHz system used a single EDO 323C transducer. The transducers are mounted in a sonar dome, 45 m forward of the drill floor, to reduce the ship-generated noise and signal attenuation from aeration beneath the hull. Both recorders were annotated automatically at fixed intervals, usually every 0.5 hr. Depth readings were taken manually every 5 min and entered into a Microsoft Excel spreadsheet.

Seismic Reflection Profiling

Available shipboard seismic sources consisted of Seismic Systems, Inc., water guns and Bolt, Inc., air guns, which have volumes in the range of 80 to 200 $in.^3$ Because of the relatively shallow, high-resolution objectives of Leg 162, one 80-$in.^3$ water gun was used as source for all the site surveys. The seismic data were recorded via a single-channel Teledyne Model 178 hydrophone streamer, containing 60 active elements over a length of 100 m. The ship's speed was held at about 6 knots (kt), and the gun and streamer were both towed at 12–18 m depth. The water-gun source was triggered from the WINFROG system at a shot interval of 8 s, equivalent to 25 m at a speed of 6 kt.

Analog data were recorded on two Raytheon Model 1807M recorders, one of which was set to a 4-s sweep ("Analog 1"), and the other set to a 2-s sweep ("Analog 2"). The signals were band-pass filtered at 18–130 Hz and 18–150 Hz for Analog 1 and Analog 2, respectively, using Krohn-Hite Model 3550 analog filters.

The seismic data were sampled at 1-millisecond (ms) sample interval and digitally recorded in SEGY format on a SUN Sparcstation 10, using the "a2d" acquisition package after application of an anti-aliasing filter with a corner frequency at 250 Hz. Seismic data were copied to both 4-mm and 8-mm DAT for each site survey. Following each survey, the data were processed using the SIOSEIS processing software package (developed at Scripps Institute of Oceanography), and displayed on an HP 650C "Design Jet" plotter. Processing steps included muting of all signals above the water-bottom, bandpass filtering between 15 and 200 Hz, running trace mix with weights of 1-2-1, and automatic gain control (AGC) using a 0.5-s window.

Magnetometer

The ship's Geometrics Model 801 proton precession magnetometer was replaced with a new Geometrics Model G-886 during the first part of Leg 162. Magnetic data were therefore acquired reliably only after 10 August, during transit from Site 985 to 986. Since then, the magnetometer was used during all transits, but not during the site surveys. The sensor was towed 500 m behind the ship, and data were recorded at 1-min intervals on the navigation files through the WINFROG software system.

Site Surveys

The grid density and seismic data quality of available pre-cruise site survey lines were highly variable from site to site. In addition, some survey lines were shot prior to availability of GPS coverage and, consequently, had less reliable navigation. Site surveys were therefore carried out at all Leg 162 sites with the exception of Site 907, which was surveyed during Leg 151 (Myhre, Thiede, Firth, et al., 1995). In addition to locating the sites accurately, the seismic data acquired during the cruise allowed us to make detailed comparisons with synthetic seismograms computed from core and downhole logging data. This enables a more reliable correlation between borehole and regional seismic data.

Each survey was designed to duplicate one of the pre-cruise survey lines and to make at least one crossing line over the proposed site, or at another potentially better site along the first survey line. Typically, the site surveys were of 10 to 20 nautical miles (nmi) in length. Exact site position was determined from GPS immediately after the survey.

Seismic Stratigraphy

Plots for seismic interpretations were made with the HP plotter using the following display parameters:

Horizontal scale: 25 traces (approximately 600 m, with a ship's speed of 6 kt) per inch (2.54 cm).
Vertical scale: 7.68 in. (19.5 cm) per second of two-way traveltime.
Positive peaks plotted to the right.

During the interpretation procedure, seismic units are defined between reflectors that either are unconformities or mark distinct changes in seismic character, or both. Because of the local character of the site surveys, the unit boundaries may not be true seismic sequence boundaries as defined by, for instance, Vail et al. (1977) and Posamentier et al. (1988). The present method has, however, proved useful when correlating the seismic stratigraphy with lithostratigraphy and physical properties. Prominent reflectors, most of which define unit boundaries, are consequently called R1, R2, etc., from top to bottom, while site-specific names have been assigned to the seismic units (e.g., GA-I for the uppermost unit at the Gardar Drift, Site 983). At Sites 982 and 986, the pre-cruise-defined regional seismic stratigraphy was adopted. For further details, see the individual site chapters in this volume.

The seismic source signature was estimated in the vicinity of some sites by stacking the seafloor reflection on 21 adjacent traces (see below). Plots of these estimated signatures (Fig. 1) show that the seismic signal varied considerably from survey to survey, probably as a result of variation in towing depth of the water gun and streamer with slight changes in ship's speed. In general, the source signature appears to have included two main peaks separated by a trough of similar amplitude, with a total length in the order of 50 ms. This is mainly a consequence of the relatively deep towing depths of both the source and receiver, and it clearly reduces the resolution of the seismic records. During interpretation, individual reflectors have been traced just above the upper positive peak. It is, however, possible that reflectors may still be 10–15 ms below the acoustic impedance contrasts that cause them.

At sites which were logged, the velocities from wireline logging are used for time-depth conversion, whereas velocities measured on cores (see "Physical Properties" section, this chapter) were used at sites were no logging was carried out. The latter velocities were corrected for core expansion upon recovery by adding 2%–5% to the velocities in the upper, nonindurated parts of the drilled sequence. Typically, this covers the APC-cored part of the sedimentary section.

Further details on the seismic data recorded at each site are given in the "Seismic Stratigraphy" sections of the site chapters in this volume.

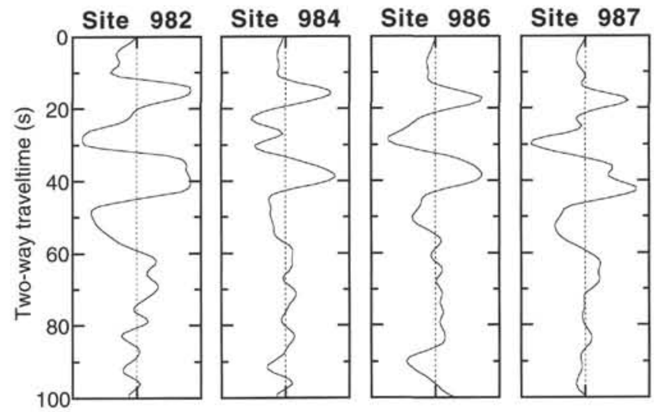

Figure 1. Seismic traces produced by stacking the seafloor reflection on 21 adjacent shots in the vicinity of Sites 982, 984, 986, and 987. Before stacking, static corrections were applied to flatten the seafloor reflection and shift its onset to 0-ms two-way traveltime. At each site the part of the trace before the fifth zero crossing (at 54–59 ms) was interpreted as representing mainly the reflection of the source signature from the seafloor.

Synthetic Seismograms

At sites where wireline logging was carried out, synthetic seismograms were generated to facilitate correlation between seismic units and core data. A synthetic seismogram is a filtered reflection coefficient series. The reflection coefficient is the ratio of the amplitude of the reflected seismic signal from an acoustic boundary to the amplitude of the incident signal. For normal incidence, the reflection coefficient of a boundary is equal to the difference between the acoustic impedance above and below it, divided by their sum. Acoustic impedance is the product of compressional velocity and bulk density. The operator used to filter the reflection coefficient series to generate a synthetic seismogram should be the same as the effective source signature of the seismic reflection data to which the synthetic seismogram is intended to be compared.

Reflection coefficients were calculated from edited sonic and density log data below 90–100 mbsf. In the uppermost 90–100 m, where log data were not available, discrete measurements of density and compressional velocity on the recovered cores were used to calculate reflection coefficients. Two-way traveltimes (TWT) were calculated by integrating the interval transit times between velocity measurements, and reflection coefficients were calculated for each 1-ms increment in TWT. In this way reflection coefficients were calculated as a function of both depth and TWT, enabling TWT on the synthetic seismogram to be related directly to depth.

Synthetic seismograms were generated for comparison with the seismic data collected in the site surveys during the leg because the data from these surveys were easily accessible in digital form. The seismic source signature of these data commonly shows lateral variation resulting from variations in the towing depth of the water gun and hydrophone streamer; therefore, it was important to estimate the source signature from the immediate vicinity of each site. The source signature at each site was estimated by applying static corrections to flatten the seafloor reflection, then stacking the 21 shots closest to the site. Amplitudes on the stacked trace typically showed a marked decrease 50–60 ms after the onset of the seafloor reflection, and the data before this TWT were interpreted as representing mainly the reflection of the source signature from the seafloor. These data were extracted and convolved with the reflection coefficient series to produce a synthetic seismogram. In areas where the seafloor is underlain by unconsolidated fine-grained sediments, this method usually produces a fairly accurate estimate of the seismic source signature because the seafloor reflection coefficient is much larger than any reflection coefficients within the sediments.

The synthetic seismogram provides insight into the causes of individual reflectors. It also allows more informal and precise correlation between the seismic reflection and core data. Such correlations are valuable for regional studies of the distribution of sediments of different ages and of lateral variations in sedimentation rates. These in turn provide additional information about depositional environments, and are also an important step in establishing how the sediment load has increased through time, its contribution to subsidence, and hence, the regional paleobathymetry. In addition to providing a useful tool for correlating core and wireline log data with regional seismic surveys and for understanding the cause of individual reflectors, synthetic seismograms are also a useful check on the velocity and density data used to produce the reflection coefficient series. If reflectors on the synthetic seismogram are similar in amplitude and shape to those on the survey data, this confirms the accuracy of local velocity and density changes. If the synthetic seismogram appears slightly expanded relative to the survey data, then the velocities used are generally lower than actual velocities; conversely, if it appears compressed, higher velocities are indicated.

COMPOSITE DEPTHS

The recovery of sequences having documented stratigraphic continuity over APC-cored intervals was crucial to the high-resolution paleoceanographic objectives of Leg 162. Drilling of multiple holes at each site ensured that intervals missing from one APC hole due to core breaks or coring disturbance were recovered in an adjacent hole. During Leg 162, as on several previous ODP legs, continuity of recovery was confirmed by development of composite depth sections and splices. The methods used on Leg 162 were similar to those used to construct composite depth sections during Leg 138 (Hagelberg et al., 1992) and Leg 154 (Curry, Shackleton, Richter, et al., 1995).

At each site, high-resolution (1- to 10-cm interval) measurements of magnetic susceptibility, GRAPE density, natural gamma radiation, and *P*-wave velocity were made on the multisensor track (MST) soon after the core sections had equilibrated to room temperature. These measurements were entered automatically into the shipboard database and minimally processed. In addition, measurements of spectral reflectance in the 650–700 nm band were made at 4- to 8-cm resolution on the split cores (see "Lithostratigraphy" section, this chapter). These parameters were then used to correlate between the different holes at each site, in order to construct a composite section and spliced record.

The need for a composite section, and thus the requisite adjustments to the meters below seafloor (mbsf) depth scale, arises from several sources (see summaries in Ruddiman et al., 1987; Farrell and Janecek, 1991; Hagelberg et al., 1992, 1995). Rebound of the sediment due to the pressure decrease during core recovery causes the cored sediment sequence to expand, relative to the in situ thickness of the drilled interval. Other factors, including variations in ship's heave not adequately absorbed by the heave compensator during drilling, can cause discrepancies between the mbsf depth and the true depth at which the core was taken. As a result, between successive cores having 100% or greater recovery, portions of the sediment sequence are commonly missing. In order to span the gaps between cores, multiple holes are required, and the core breaks must be staggered so that material missing at one core break is available in another hole.

A composite section and a splice were developed for each site drilled during Leg 162, using an interactive program developed for this task by the Borehole Research Group of Lamont-Doherty Earth Observatory, and patterned after the Leg 138 correlation software. First, the magnetic susceptibility, GRAPE, natural gamma radiation, and spectral reflectance data for the holes at each site were examined. One data set, with the most visually distinctive and highest amplitude variations, was chosen for primary use in correlation. This data set, typically magnetic susceptibility, was plotted on the screen for all of the holes at the site simultaneously. We chose the hole which appeared to have the best recovery of the sediment-water interface. The top core in that hole became the "anchor" for the composite section.

By visually comparing the plotted data for this core with the data for the uppermost core in one of the other holes, we could recognize distinctive sedimentary features present in both cores. We then graphically selected a feature in the "anchored" core, and the same feature in the other core, and created a tie line between them. The depth of the second core was then adjusted, in order to align the distinctive features in both at exactly the same depth. This process was repeated for the uppermost core from the other holes, so that the sedimentary features in the uppermost cores were all at the same "composite" depth.

Another distinctive feature was then chosen, which was visible near the bottom of one of the adjusted cores, and also present in the top of one of the underlying cores. A tie line was created between correlative features and the new lower core was moved so that the features were in alignment. Moving back and forth between all the holes at each site (commonly three), we worked down the sedimentary section, adjusting the depth of each core in order to align its sedimentary features with the correlative ones in the other cores. Mathematical cross-correlations between selected segments of the data were calculated where needed to confirm our visual correlations. As each core was moved, all the cores beneath it were moved with it. The new adjusted depths, or "composite" depths, were appended as an additional column to the original data file.

After making a preliminary composite section as described above using one data set, the new composite depth scale was applied to another data set. We would then repeat the process as above, plotting on the screen the new data set for each hole, and then working down from the sediment-water interface. The position of each core was examined and minor adjustments were made where necessary to ensure that sedimentary features were aligned as well as possible.

Perfect alignment of all features was not possible, because of slight expansion or compaction of the sediments during the coring process. We did not adjust relative depths *within* any cores: that is, we did not stretch or compress any individual cores, but changed only the distances between them at core breaks. Therefore, there are cases in which a small range of relative alignments between two cores would be equally acceptable. Any decisions about final small-scale placement of the cores were made by considering the best locations for splice tie points, as discussed below.

The resulting composite depth scale is presented in each chapter (see, for example, table 4, "Site 980/981" chapter, this volume). The tables include the original (mbsf) depth of the top of each section, the new composite depths (mcd), and the offset between the two, which can be used to convert from mbsf to mcd values.

The next step in the process was to create a "splice" suitable for high-resolution sampling, and for analysis of the MST and spectral reflectance data. Each splice was designed to comprise an uninterrupted sedimentary sequence for a site and to provide a single representative record of each lithologic parameter or physical property (susceptibility, natural gamma radiation, GRAPE, and spectral reflectance). To make the splice, we began with the composite section, which was developed as described above, and used the same software package to manipulate the data sets graphically on the screen. We first selected the core with the sediment-water interface used to anchor the composite. We then chose a deeper point in that core which was aligned perfectly with the same precisely identifiable feature in a core in another hole. In order to be useful, the second core also had to extend deeper than the first. A splice tie line was created between the two cores at the particular composite depth of the feature chosen.

The process was then repeated, by selecting a point lower in the second core, with a suitable correlative tie point at the same mcd in another hole. The splice was thus extended downward by moving from hole to hole, bridging the gaps in the sedimentary sequence at the core breaks. Intervals that included large dropstones, were disturbed during drilling, or were heavily sampled for shipboard studies were avoided where possible in the splice. Since there can be considerable stretching and/or compression of an interval in one core compared to the same interval in another core, the exact length of the splice depends on the portions of cores selected to build it. The tie points that describe the splices are given in each site chapter (see, for example, table 4, "Site 980/981" chapter, this volume).

The need for a composite section and a splice to verify stratigraphic continuity is illustrated in Figure 2. In the left-hand panel, magnetic susceptibility data from the three holes at Site 981 are shown on the initial, mbsf depth scale. In the middle panel, the same records are shown after the depth scale has been adjusted to align correlative features as described above. Gaps are evident at the core breaks, such as between Cores 162-981B-6H and 7H. In the right-hand panel, the splice constructed for this interval is shown. Because there are gaps in the sequence even between cores with 100% recovery, the composite section "grows" downhole relative to the mbsf scale, typically on the order of 10%. The growth of each composite section is shown in each chapter (see, for example, fig. 4, "Site 980/981" chapter, this volume).

The splices are precise to 10 cm or less, depending on the resolution of the data used in choosing the tie points. Sliding or disturbance of the sediment in the core liner during splitting would decrease the precision of the splice. The quality of the correlations between the tie points is also important. In intervals where none of the lithologic parameters could provide precise, unambiguous correlations, the composite was discontinued, and no additional depth adjustments were made below that point. The composite depth sections therefore typically extend only to the base of multiple cored intervals, usually the APC intervals. At sites having deep sequences singly drilled by XCB or RCB, where relative offsets could not be determined, no additional

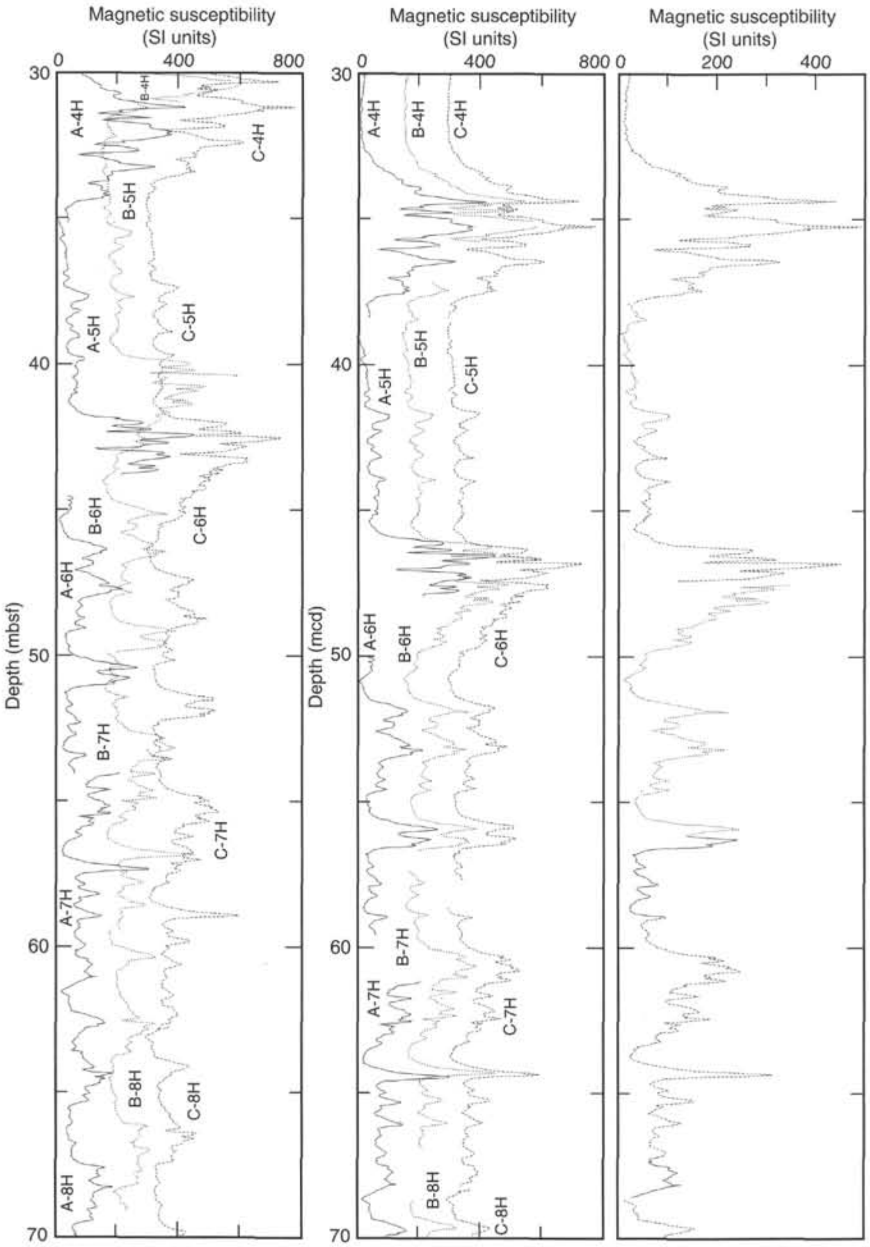

Figure 2. Portions of the magnetic susceptibility records from Site 981. Left: Cores 162-981A-4H through 7H (solid line), 162-981B-4H through 8H (dotted line), and 162-981C-4H through 8H (dashed line) on the meters below seafloor (mbsf) depth scale. Data from each hole are offset for clarity. Middle: The same cores on the meters composite depth (mcd) scale. The composite depth section has the advantage that features common to all holes are in relative alignment. Right: Corresponding portion of the spliced magnetic susceptibility record assembled from the same cores.

depth adjustments were made, and in the splices each successive core was simply appended to the next, preserving the original mbsf depths with the accumulated mcd offset added. Therefore, the lower portions of the spliced records at those sites may contain intervals of nonrecovery or disturbance.

LITHOSTRATIGRAPHY

Visual Core Description

Sediment "Barrel Sheets"

The core description forms (Fig. 3), or "barrel sheets," summarize the data obtained during shipboard analysis of each sediment core. The following discussion explains the ODP conventions used for compiling each part of the core description forms and any exceptions to these procedures adopted by the Leg 162 scientific party.

Shipboard scientists were responsible for visual core logging, smear-slide analyses, thin-section descriptions, and color analysis. Biostratigraphic (age), geochemical ($CaCO_3$, pore-water chemistry), physical property (wet bulk density, shear strength, magnetic susceptibility, and natural gamma-ray measurements), and X-ray diffraction data were integrated with other sedimentological information to augment visual core descriptions.

Core Designation

Cores are designated using leg, site, hole, core number, and core type as discussed in a preceding section (see "Core Handling Procedures" section, this chapter). The cored interval is specified in terms of meters below seafloor (mbsf). When necessary for interhole and/or intersite comparison, lithostratigraphic data are presented vs. meters composite depth (mcd; see "Composite Depths" section, this chapter).

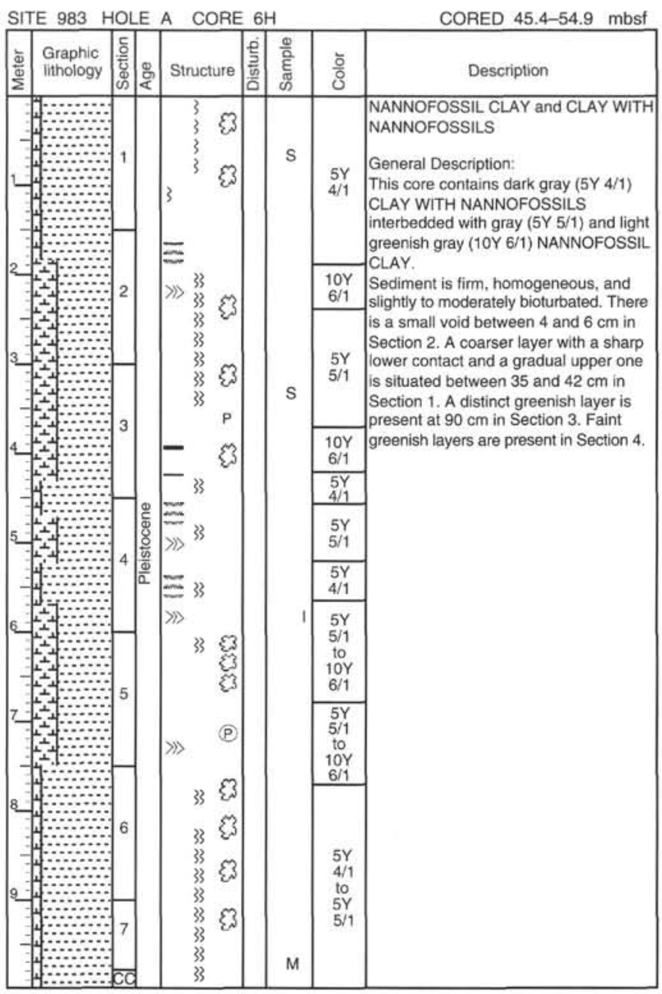

Figure 3. Example of a core description form ("barrel sheet") used for sediments and sedimentary rocks in cores recovered during Leg 162. Keys to symbols are presented in Figures 4 and 5.

Chronostratigraphy

The chronostratigraphic unit, as recognized on the basis of paleontological and paleomagnetic criteria, is shown in the "Age" column on the core summaries. The zonations and ages used during Leg 162 are presented in the "Biostratigraphy" section (this chapter). Boundaries between assigned ages were indicated as follows:

1. Sharp boundary: straight line.
2. Unconformity or hiatus: line with plus signs above it.
3. Uncertain: line with question marks.

Graphic Lithology Column

The lithology of the material recovered is represented on the core description forms by up to three symbols in the column titled "Graphic Lithology" (Figs. 3, 4). Where an interval of sediment or sedimentary rock is a homogeneous mixture, the constituent categories have been separated by a solid vertical line, with each category represented by its own symbol. Constituents accounting for <10% of the sediment in a given lithology are not shown in the "Graphic Lithology" column. In an interval comprising two or more sediment lithologies that have different compositions, and that are thinly interbedded, the average relative abundances of the lithologic constituents are represented graphically by dashed lines that vertically divide the interval into appropriate fractions, as described above. The "Graphic Lithology" column shows only the composition of layers or intervals exceeding 20 cm in thickness.

Sedimentary Structures

In sediment cores, natural structures and structures created by the coring process can be difficult to distinguish. Natural structures observed are indicated in the "Structure" column of the core description form (Fig. 3). The column is divided into three vertical areas for symbols. The symbols on the outer portions of the "Structure" column indicate the location of sediment features such as primary sedimentary structures, discrete trace fossils, soft-sediment modification features, structural features, and diagenetic features. The intensity of bioturbation is shown in the central portion of the "Structure" column of the barrel sheet in the conventional manner (slight, moderate, and heavy). Leg 162 sedimentologists recognize that homogeneous sediment may be the product of deposition of material of homogeneous color and grain size, resulting in sediment having no observable lamination or color change, or it may be the product of total mixing by the action of bioturbating organisms. Since it is impossible to distinguish between these two causes, no bioturbation is indicated. Color banding symbols appear in the outer portion to indicate both color banding and interbedded lithologies, because the latter was invariably accompanied by color changes. The symbols used to describe each of these biogenic and physical sedimentary structures are shown in Figure 5.

Sedimentary Disturbance

Deformation and disturbances of sediment that clearly resulted from the coring process are illustrated in the "Drilling Disturbances" column (Fig. 3) using symbols shown in Figure 5. Blank regions indicate the absence of drilling disturbance. The degree of drilling disturbance is described for soft and firm sediments using the following categories:

1. Slightly deformed: bedding contacts were slightly bent.
2. Moderately deformed: bedding contacts were extremely bowed.
3. Highly deformed: bedding was completely disturbed, in some places showed symmetrical diapir-like or flow structures.
4. Soupy: intervals were water-saturated and had lost all aspects of original bedding.

The degree of fracturing in indurated sediments was described using the following categories:

1. Slightly fractured: core pieces were in place and contained little drilling slurry or breccia.
2. Moderately fragmented: core pieces were in place or partly displaced, but the original orientation was preserved or recognizable (drilling slurry may surround fragments).
3. Highly fragmented: pieces were from the cored interval and probably in the correct stratigraphic sequence (although they may not represent the entire section), but the original orientation was completely lost.
4. Drilling breccia: core pieces have lost their original orientation and stratigraphic position, and may have been mixed with drilling slurry.

Color and Spectral Reflectance

The hue and chroma attributes of color were determined using the Minolta CM-2002 hand-held spectrophotometer as soon as possible

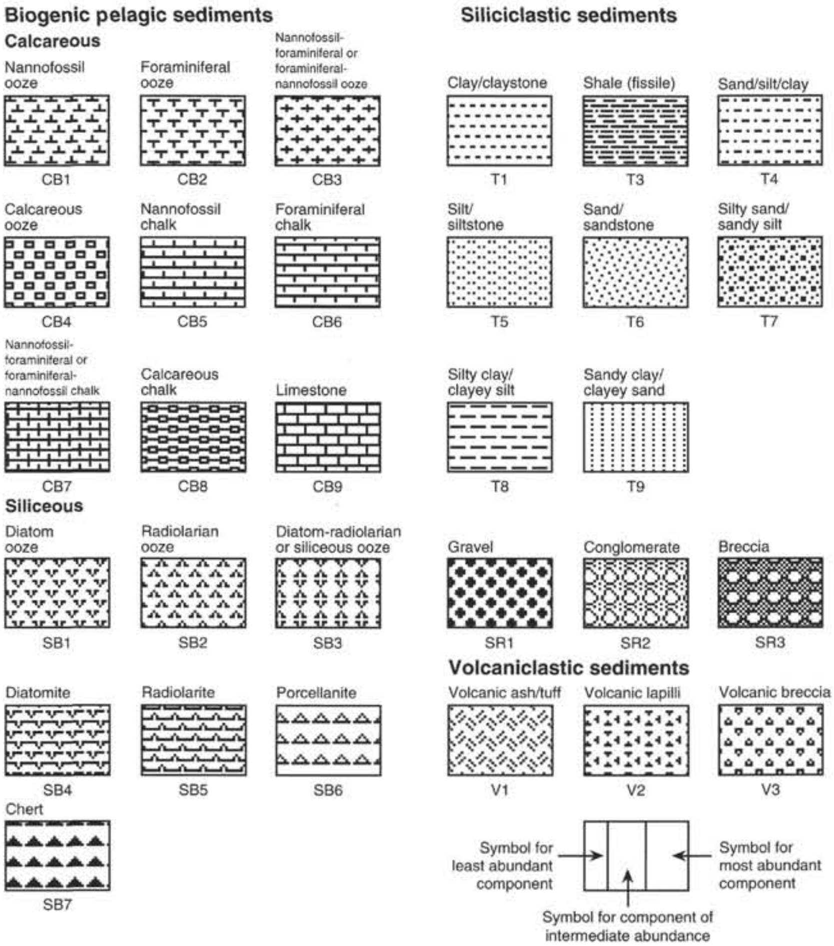

Figure 4. Key to symbols used in the "Graphic Lithology" column of the core description forms.

after the cores were split, as redox-associated color changes may occur when deep-sea sediments are exposed to the atmosphere. Core color, in standard Munsell notation, is given in the "Color" column on the core description form.

The OSU Spectral Reflectometer, designed by Alan Mix, William Rugh, and Sara Harris, was used to make detailed systematic measurements of the relative spectral reflectance of the sediments. The instrument consists of a computer-controlled, motorized track assembly that advances a core section into sampling position under a commercially available light integration sphere. The integration sphere is brought into contact with the sediment via a computer-controlled, vertical stepping motor. Temperature, conductivity and strain sensors detect contact with the sediment surface. Light, with known spectral characteristics passing through fiber optics, is steered using a directional mirror toward two reference ports and a sample port during each measurement. The light that is diffusely reflected off the sediments is integrated within the sphere and then split into constituent wavelengths by a diffraction gradient and collected with a multichannel detector.

An earlier version of this instrument was employed during Leg 138 (see Mix et al., 1992). The current version was used for post-cruise analysis of cores collected during Leg 154. The new design has incorporated four improvements: (1) addition of the integration sphere, (2) use of a motorized mirror for source beam direction, rather than a source beam splitter, (3) determination of internal "white" reference and "black" background estimations for each sample measurement within a section, and (4) extension of the spectral range of the instrument beyond the visible spectrum to include both ultraviolet (UV) and near-infrared (nIr) wavelengths. These improvements have increased the signal-to-noise ratio considerably over the earlier version of the instrument.

Reflected light was measured in 1024 0.628-nm-wide bands ranging from 250 to 950 nm. These measurements were taken at 8-cm intervals, and in some cases, at higher resolution (4-cm intervals) on all APC and some XCB cores from one designated hole (usually the "A" hole) at each site, and on chosen intervals from the other holes at each site. For shipboard analysis, the raw data was converted to percentage of reflectance and averaged into four 50-nm-wide bands defined as ultraviolet (250–300 nm), blue (450–500 nm), red (650–500 nm), and near infra-red (800–950 nm). As an aid to defining lithostratigraphic units we employed the red band, which is near the instrument's maximum response. This band was also used as an aid in constructing composite sections (see "Composite Depths" section, this chapter). For comparison to shipboard measurements of the carbonate content of sediment, the blue band was used (carbonate has a somewhat higher reflectance at this wavelength than at longer wavelengths; see Mix et al., 1992).

Samples

The position of samples taken from each core for shipboard analysis is indicated in the "Samples" column on the core description form, as follows:

I = interstitial-water sample.
M = micropaleontology sample.
S = smear slide.

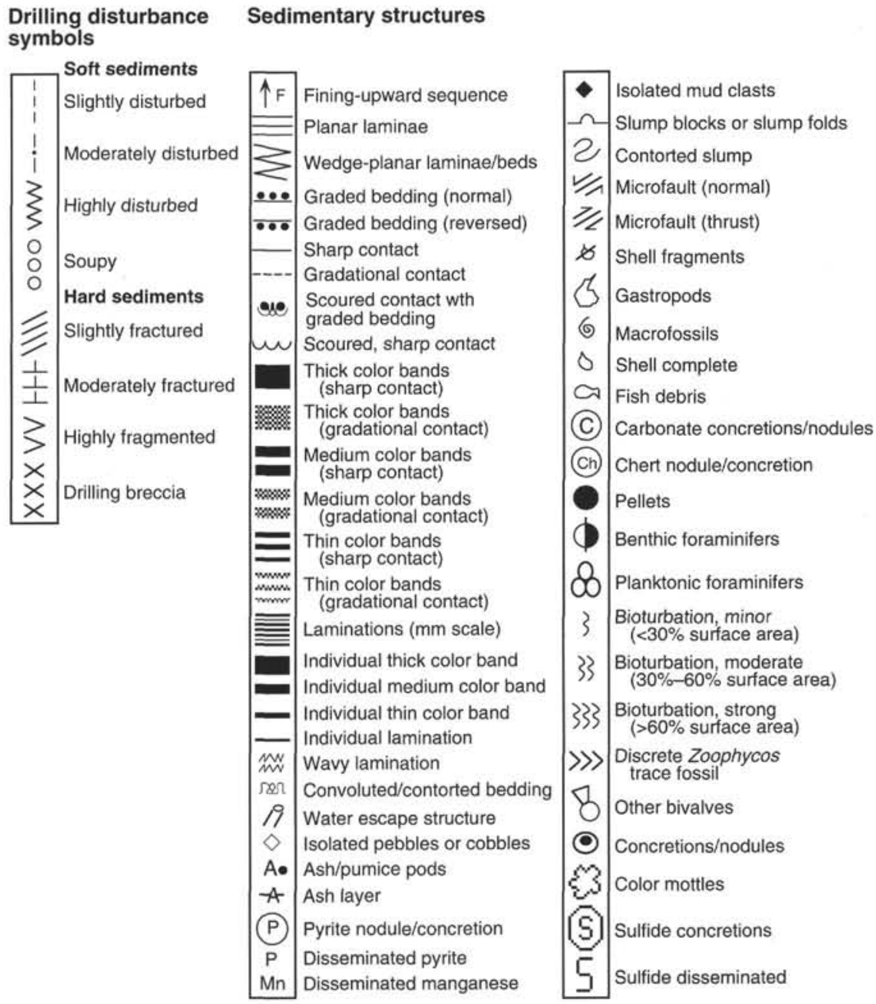

Figure 5. Left-hand column: Key to symbols used in the "Disturbance" column of the core description forms. Middle and right-hand columns: Key to symbols used to indicate color banding, bioturbation, and isolated sedimentary structures/trace fossils/macrofossils in the "Structure" column of the core description forms.

Smear-Slide Summary

Tables that summarize data from smear-slide analyses appear in Section 4 near the back of this volume. These tables include information on the sample location, whether the sample represents a dominant ("D") or a minor ("M") lithology in the core, and the estimated percentages of sand, silt, and clay, together with all identified components. The subjective nature of these data should be kept in mind, even though they were produced by a smear-slide specialist. Carbonate percentage data and color data were used as aids in determining relative proportions of pelagic and siliciclastic components whenever possible.

Lithologic Description Text

The lithologic description text that appears on each core description form (barrel sheet) consists of two parts: (1) a heading that lists all the major sediment lithologies observed in the core and (2) a general description of these sediments, including location of significant features in the core and a subjective index of the contrast in color banding in the core. Descriptions and locations of dropstones, concretions, thin interbedded lithologies, and other minor lithologies are included in the text, as is any clarifying information regarding sediment disturbance produced by drilling/coring or natural processes.

Classification of Sediments and Sedimentary Rocks

We have followed the classification procedures suggested by Mazzullo et al. (1988). The sediments on Leg 162 are composed of pelagic and siliciclastic components, according to this classification scheme. The pelagic component is usually composed of the skeletal debris of open-marine calcareous, and to a lesser extent, siliceous microfauna (e.g., foraminifers and radiolarians, respectively) and microflora (e.g., calcareous nannofossils and diatoms, respectively) and associated organisms. The siliciclastic component is composed of mineral and rock fragments derived from igneous, sedimentary, and metamorphic rocks. The relative proportions of the two components are used to define the major classes of "granular" sediments encountered. Thus, pelagic sediments are composed of >60% biogenic grains, and siliciclastic sediments are composed of >60% siliciclastic grains (Mazzullo et al., 1988). Mixed sediments contain proportions of these two grain types between 40% and 60%.

Classification of Granular Sediment

A granular sediment may be classified by designating a principal name and major and minor modifiers (Mazzullo et al., 1988). The principal name of a granular sediment defines its granular sediment class (see above); the major and minor modifiers describe the texture, composition, fabric, and/or shape of the grains themselves (Table 1).

Table 1. Outline of the sediment classification scheme used by Mazzullo et al. (1988) for pelagic and siliciclastic sediments and sedimentary rocks.

Sediment class	Major modifier	Principal names	Minor modifiers
Pelagic	1. Composition of biogenic and neritic grains present in major amounts 2. Texture of clastic grains present in major amounts	1. Ooze 2. Chalk 3. Limestone 4. Radiolarite 5. Diatomite 6. Spiculite 7. Chert	1. Composition of biogenic grains present in minor amounts 2. Texture of clastic grains present in minor amounts
Siliciclastic	1. Composition of all grains present in major amounts 2. Grain fabric (gravels only) 3. Grain shape (optional) 4. Sediment color (optional)	1. Gravel 2. Sand 3. Silt 4. Clay (etc.)	1. Composition of all grains present in minor amounts 2. Texture and composition of siliciclastic grains present as matrix (for coarse-grained clastic sediment)

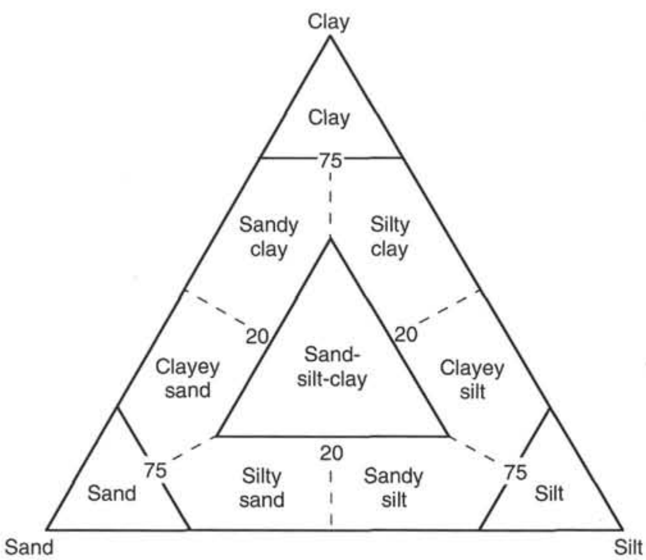

Figure 6. Ternary diagram showing principal names for siliciclastic sediments (from Mazzullo et al., 1988).

Principal Names

Each granular sediment class has a unique set of principal names, which are outlined in Table 1.

For pelagic sediment, the principal name describes the composition and degree of consolidation using the following terms:

1. Ooze: unconsolidated calcareous and/or siliceous biogenic sediments.
2. Chalk: firm biogenic sediment composed predominantly of calcareous biogenic grains.
3. Limestone: hard pelagic sediment composed predominantly of calcareous pelagic grains.
4. Radiolarite, diatomite, and spiculite: firm pelagic sediment composed predominately of siliceous radiolarians, diatoms, and sponge spicules, respectively.
5. Chert: hard pelagic sediment composed predominately of siliceous pelagic grains.

For siliciclastic sediment, the principal name describes the texture and is assigned according to the following guidelines:

1. The Udden-Wentworth grain-size scale (Wentworth, 1922) defines the grain-size ranges and the names of the textural groups (gravel, sand, silt, or clay) that are used as the principal names of siliciclastic sediment.
2. When two or more textural groups are present in a siliciclastic sediment in sufficient amounts, they are listed as principal names in order of increasing abundance in accordance with the ternary diagram presented in Figure 6.
3. The suffix "stone" is affixed to the principal names sand, silt, and clay when the sediment is lithified.

Major and Minor Modifiers

The principal name of a granular sediment class is preceded by major modifiers and is followed by minor modifiers (preceded by the term "with") that describe the lithology of the granular sediment in greater detail (Table 1). The most common use of major and minor modifiers is to describe the composition and textures of grain types that are present in major (>25%) and minor (10%–25%) proportions. Note that the major modifiers are always listed in order of increasing abundance. As an example, an unconsolidated pelagic sediment containing 30% clay, 15% foraminifers, and 55% nannofossils would be called a clayey nannofossil ooze with foraminifers (Mazzullo et al., 1988). The minor modifiers are listed in order of decreasing abundance.

Glaciogenic Sediments

Visually distinctive glaciogenic sediments are relatively common in Leg 162 sediments, particularly ice-rafted debris. These sediments are described using the classification for siliciclastic sediments. They are often identified by the presence of isolated angular dropstones in the midst of fine-grained sediments, as dropstone clusters, or as dropstones with other coarse-grained sediments. Characteristics of these sediments are detailed on the core description forms (barrel sheets) within the "General Description" portion of the lithologic description text.

BIOSTRATIGRAPHY

Introduction and Time Scale

Preliminary age determinations of Leg 162 sediments are based on biostratigraphic analysis of calcareous and siliceous microfossils. Calcareous groups analyzed include calcareous nannofossils, planktonic and benthic foraminifers, and *Bolboforma.* Siliceous biostratigraphy includes analysis of diatoms, siliceous flagellates, and radiolarians. Age assignments were made primarily on core-catcher samples, but additional samples from key intervals were used to refine the biostratigraphy.

Biostratigraphic zonal assignments established for the various fossil groups studied during Leg 162 are correlated to the geomagnetic polarity time scale when possible (see "Paleomagnetism" section, this chapter). Biostratigraphic datums were assigned numerical ages based on the time scale of Cande and Kent (1995). Placement of epoch/subepoch boundaries relative to magnetic chrons and biostratigraphic zones mainly followed Berggren et al. (1985, 1995), while numerical ages followed Cande and Kent (1995) (Table 2).

During shipboard study, biostratigraphic assignments from Leg 162 were based on previously established biostratigraphic zonations for the North Atlantic and the Norwegian Sea where possible. Difficulties such as variable preservation, low abundances, endemism,

Table 2. Epoch and subepoch boundaries correlated to magnetic chrons and nannofossil zones.

Boundary	Age (Ma)	Boundary criterion
late/middle Pleistocene	0.78	Brunhes/Matuyama boundary
Pleistocene/Pliocene	1.77	Top of Olduvai, approximated by nannofossil Zone CN13a/CN13b boundary (1.79 Ma)
late/early Pliocene	3.58	Base of Subchron C2An.3n, approximated by nannofossil Zone CN11/CN12 boundary (3.75 Ma)
Pliocene/Miocene	5.30	Within Subchron C3r, approximated by nannofossil Zone CN9/CN10 boundary (5.60 Ma)
late/middle Miocene	10.95	Base of Subchron C5n.2n, approximated by nannofossil Zone CN5/CN6 boundary (11.20 Ma)
middle/early Miocene	16.01–16.29	Within Subchron C5Cn.1n, approximated by nannofossil Zone CN3/CN4 boundary (16.0 Ma)

Note: Ages based on Cande and Kent (1995).

and possible diachrony sometimes hindered correlation of Leg 162 fossil assemblages to fossil zones defined from lower latitudes.

Calcareous Nannofossils

Calcareous nannofossil zones are given in the widely used zonation of Okada and Bukry (1980) wherever possible. Smear slides are prepared directly from unprocessed samples and examined with a light microscope at a magnification of about 1000×. Abundance of calcareous nannofossils is estimated as follows:

V (very abundant) = >50 specimens per field of view.
A (abundant) = 10–50 specimens per field of view.
C (common) = 1–9 specimens per field of view.
F (few) = 1 specimen per 2–50 fields of view.
R (rare) = 1 specimen per 51–200 fields of view.

The qualitative evaluation of the preservation of calcareous nannofossils is recorded as

G (good) = specimens exhibit little evidence of dissolution and/or overgrowth.
M (moderate) = specimens exhibit moderate dissolution and/or overgrowth; a significant proportion (up to 20%) of the specimens cannot be identified to species with absolute certainty.
P (poor) = specimens exhibit severe dissolution and/or overgrowth; more than 20% of the specimens cannot be identified at the species level.

Foraminifers

The classic planktonic foraminifer "N" (Neogene) zones of Blow (1969, 1979), established for tropical regions, have limited value in middle and high latitudes because many of the warm-water forms on which these zonations are based are not found at higher latitudes. The temperate zonation of Berggren et al. (1983) also has limited value for the same reason. In the modern ocean, the vast majority of planktonic foraminifer species live in tropical and subtropical waters, with species richness decreasing markedly toward polar waters. The North Atlantic and Norwegian-Greenland Sea region sampled during Leg 162 ranges from temperate to polar waters. Zonations for this region are largely based on species within the genus *Neogloboquadrina* (Berggren, 1972; Weaver and Clement, 1986; Hooper and Weaver, 1987; Spiegler and Jansen, 1989). Planktonic foraminifer biostratigraphy here is based mainly on two different zonation schemes, one for the North Atlantic (Weaver and Clement, 1986) and one for the Norwegian-Greenland Sea (Spiegler and Jansen, 1989).

The temperate zonation for the northern North Atlantic (Weaver and Clement, 1986, 1987) is used for Sites 980/981, 982, 983, and 984. In the lower and middle Miocene at Site 982, the temperate zonation of Berggren et al. (1983) is applicable (see "Biostratigraphy" section, "Site 982" chapter, this volume). The subpolar zonation for the Norwegian-Greenland Sea (Spiegler and Jansen, 1989) is used for Sites 907, 985, 986, and 987. Age assignments of specific planktonic foraminifer datums are from Weaver and Clement (1986), Raymo et al. (1989), and Berggren et al. (1985, 1995).

Benthic foraminifers provide limited biostratigraphic age control as currently applied to Leg 162 samples and, with the exception of Site 985, all zones recognized are local assemblage zones. The agglutinated benthic foraminiferal zonation of the lower sequence of Site 985 is based on Kaminski et al.'s (1990) zonation of ODP Site 643; the latter is constrained by palynomorph biostratigraphy from that site (Manum et al., 1989) and correlation with the dinocyst zones of Williams and Bujak (1985). Additionally, individual benthic foraminiferal datums are recognized and discussed for each site. Particularly useful, but requiring further study, is the last occurrence of *Stilostomella lepidula* at about 0.9 Ma; Thomas (1987) noted that the last appearance of *Stilostomella* spp. at Deep Sea Drilling Project (DSDP) Site 610 occurs at about 45 mbsf (less than 1 Ma), considerably younger than at deeper North Atlantic sites. Other age-diagnostic taxa which might be useful for regional biostratigraphic correlation purposes include the last occurrences of *Ehrenbergina trigona, Laticarinata pauperata,* and *Siphonia tenuicarinata,* and the first occurrence of *Cibicidoides wuellerstorfi,* all of which are recorded at Site 982.

In addition, benthic foraminifers have provided an important means of recognizing downslope transportation and reworking of shelf and upper slope assemblages. For example, the increased abundance of the ubiquitous and often highly abundant upper slope and shelf species *Elphidium excavatum* through the Quaternary sequence of Site 984 may indicate more extensive glaciation of the Icelandic shelves at this time.

To obtain planktonic and benthic foraminifers from core-catcher samples, a 10-cm^3 sample was disaggregated and washed over a 63-μm sieve. Between samples, sieves were soaked in a solution of Methylene Blue carbonate stain to identify potential contamination. A variety of methods were used for disaggregation including ultrasonic treatment and hot Calgon solution for consolidated sediments. The sample was dried, and benthic and planktonic foraminifers were examined under the binocular microscope and identified, where possible, to species level. *Bolboforma* genera were also noted (see below). Species abundances were recorded as

D (dominant) = >60%.
A (abundant) = 30%–60%.
C (common) = 10%–30%.
F (few) = 5%–10%.
R (rare) = 1%–5%.
T (trace) = <1%.
B (barren) = no specimens observed.

Preservation was categorized as G (good), M (moderate), and P (poor).

Bolboforma

The *Bolboforma* zonation may have the potential to become a useful supplementary biostratigraphic tool in the Cenozoic middle and higher latitude calcareous sediments. *Bolboforma* have been found in numerous DSDP and ODP sites. Thirteen zones were established for the middle Eocene to upper Pliocene (Spiegler and von Daniels, 1991). Seven of these zones were recognized in the Norwegian Sea (Qvale and Spiegler, 1989). Cenozoic *Bolboforma* zonations that have been calibrated to calcareous nannofossil stratigraphy and magnetostratigraphy have been published on North Atlantic sites (Spiegler and Müller, 1992) and on subantarctic Atlantic ODP Leg 114 (Kennett and Kennett, 1991; Spiegler, 1991). A revision of the upper/middle Miocene boundary on the Vøring Plateau (ODP Leg 104), according to calcareous nannofossils and *Bolboforma,* is given by Müller and Spiegler (1993). *Bolboforma* calcified their tests under temperate to cold conditions and are indicative of subarctic/subantarctic to transitional water masses.

The preparation methods used to obtain *Bolboforma* were the standard techniques used for foraminifers described above. The occurrences of *Bolboforma* specimens are designated as

R (rare) = 1–10 specimens per 10-cm^3 sample.
C (common) = 11–25 specimens per 10-cm^3 sample.
A (abundant) = more than 25 specimens per 10-cm^3 sample.

Diatoms

The Norwegian-Greenland Sea and the North Atlantic are paleoenvironmentally distinct regions. While diatom assemblages found in sediments from the North Atlantic contain many species typically seen in open-ocean sediments, diatom assemblages from the Norwegian-Greenland Sea contain many neritic forms restricted to the continental shelves. Constructing a diatom zonation for the Norwegian-Greenland Sea which is easily correlated to other zonations has been an ongoing problem for researchers studying the northern North Atlantic.

Early DSDP studies on diatoms from the Norwegian-Greenland Sea led to the construction of zonations by Schrader and Fenner (1976) and Dzinoridze et al. (1978). Norwegian-Greenland Sea diatom biostratigraphy for Leg 162 is based on these early zonal schemes. In addition, studies by Bodén (1992) for the Norwegian Sea established chronostratigraphic control for several of the upper Neogene diatom datums that are used.

Biostratigraphy of the North Atlantic was determined using the North Atlantic zonation of Baldauf (1984, 1987). Biostratigraphic studies completed by Barron (1985, 1992) and Barron and Gladenkov (1995) from the North Pacific and the low-latitude Pacific, which contain many of the same open-ocean diatom species found in the North Atlantic, are also useful for Leg 162 diatom biostratigraphy. The correlation of early Miocene to Holocene diatom zonations from the Norwegian-Greenland Sea and the North Atlantic to the magnetic polarity time scale of Cande and Kent (1995) is shown in Figure 7.

Smear slides were prepared from all core catchers during the cruise. Diatom abundance was determined based on smear-slide evaluation at 400×, using the following means of estimating abundance:

A (abundant) = >6 diatoms per field of view.
C (common) = 1–5 diatoms per field of view.
F (few) = 1–4 diatoms per 5 fields of view.
R (rare) = 1–10 diatoms per horizontal traverse (54 fields of view).
T (trace) = <5 whole diatoms per slide, fragments present,
B (barren) = no identifiable diatoms or diatom fragments.

If diatoms were not abundant enough in smear slides to be biostratigraphically useful, samples were processed as follows: 1–2 cm^3 of sediment was treated with hydrochloric acid. The sample was then mixed with 10% hydrogen peroxide until disaggregated. It was subsequently washed by repeated centrifuging at 2000 rpm for 3 min before decanting, until liquid had a pH of approximately 6. Qualitative strewn slides of the cleaned samples were prepared from subsamples drawn by micropipet, and mounted on cover glasses using Norland

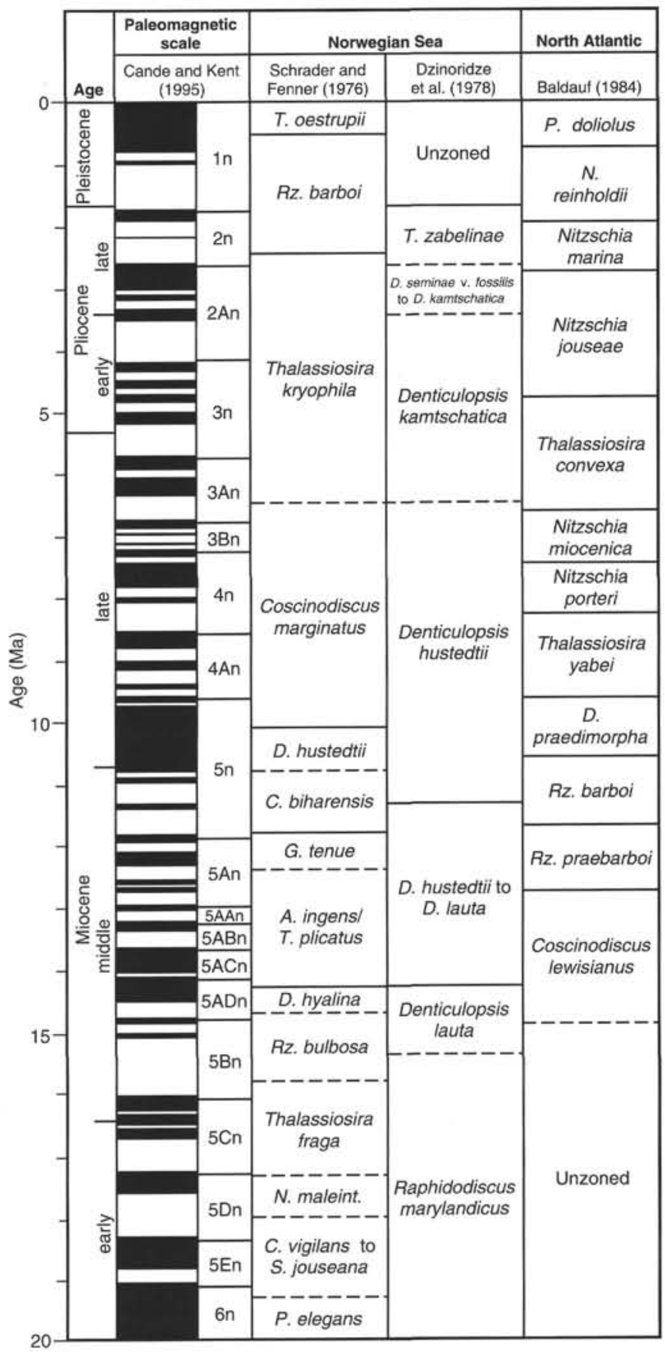

Figure 7. Early Miocene to Holocene diatom biostratigraphic zonations for the North Atlantic and Norwegian-Greenland Sea, as compiled by Baldauf (1984). Chronostratigraphic calibration is to the magnetostratigraphic time scale of Cande and Kent (1995).

Optical Adhesive. Samples with abundant clay and rare diatoms were washed using a 2-µm sieve, which biases assemblages toward larger diatoms but improves the chances of successful biostratigraphy on diatom-poor sediments. All slides were examined using 40× (dry), 63× (oil), and 100× (oil) objectives.

Qualitative estimates of abundance of individual diatom taxa are based on the number of specimens observed per field of view using the 63× objective, and are recorded as follows:

A (abundant) = 2 or more specimens per field of view.
C (common) = 1–2 specimens per field of view.
F (few) = 2–10 specimens per horizontal traverse.
R (rare) = 1 specimen per horizontal traverse.
T (trace) = single specimen or fragment observed.

Estimation of diatom preservation was determined qualitatively and recorded as follows:

G (good) = both finely silicified and robust forms present; no significant alteration of frustules observed, except for minor fragmentation.
M (moderate) = some finely silicified forms present; some alteration present.
P (poor) = finely silicified forms rare or absent; assemblage dominated by robust forms and fragments.

Siliceous Flagellates

Smear slides prepared from unprocessed bulk sediment were analyzed for biostratigraphically significant siliceous flagellates, including silicoflagellates, ebridians, and actiniscidians. Preliminary taxonomic and stratigraphic investigations mainly followed the studies of Martini and Müller (1976) and Perch-Nielsen (1978) from DSDP Leg 38, Martini (1979) and Bukry (1979) from DSDP Leg 49, Locker and Martini (1989) from ODP Leg 104, and Locker (in press) from ODP Leg 151. Additional information was taken from Perch-Nielsen (1985).

The silicoflagellate and ebridian/actiniscidian zonations applied during Leg 162 generally correspond to those of Leg 104. Only one exception was made: for the middle to late Miocene time interval an *Actiniscus tetrasterias* Zone was used within the ebridian/actiniscidian zonation, because other indicative ebridian/actiniscidian species could be not found.

Slides were prepared as follows: bulk sediment particles were strewn on cover glasses 22 × 30 mm in size and covered with Norland Optical Adhesive. The slides were then scanned with a magnification of 400×. Siliceous flagellate abundances were classified as

A (abundant) = >10 specimens per traverse.
C (common) = 4–10 specimens per traverse.
F (few) = 2–3 specimens per traverse.
R (rare) = 1 specimen per traverse.
T (trace) = <1 specimen per traverse or fragments only.
B (barren) = no silicoflagellate skeletons or fragments.

The preservation of skeletons was recorded as

G (good) = specimens are not fragmented or corroded.
M (moderate) = specimens show minor signs of fragmentation or corrosion.
P (poor) = specimens are fragmented or strongly corroded.

Radiolarians

Suspension slides prepared from decalcified and sieved sediment were investigated for biostratigraphically significant radiolarians. Since no appropriate radiolarian zonation is available for the Neogene of the high northern Atlantic at present, age information was taken from different sources, particularly from Goll and Bjørklund (1989) and Nigrini and Sanfilippo (1992). Goll and Bjørklund (1989) provide a radiolarian zonation for the Norwegian-Greenland Sea, and Nigrini and Sanfilippo (1992) provide one for the mid latitudes, particularly for the Pacific Ocean.

Preliminary taxonomic and stratigraphic investigations followed also the studies of Bjørklund (1976) for DSDP Leg 38, Westberg-Smith and Riedel (1984) for DSDP Leg 81, and Lazarus and Pallant (1989) for ODP Leg 105. Additional taxonomic information was obtained from Nigrini and Moore (1979), Nigrini and Lombari (1984), and Takahashi (1991).

Slides were prepared as follows: bulk sediment samples were treated with hydrogen peroxide and hydrochloric acid, accompanied by heating. After sieving at 45 μm, particles were strewn on slides, covered with Norland Optical Adhesive,. and protected with a cover glass 22 × 40 mm in size. Slides were then scanned with a magnification of 200×. Radiolarian abundances were classified as

A (abundant) = >100 specimens per traverse.
C (common) = 51–100 specimens per traverse.
F (few) = 11–50 specimens per traverse.
R (rare) = 1–10 specimens per traverse.
T (trace) = <1 specimens per traverse or a few fragments only.
B (barren) = no radiolarian skeletons or fragments.

The preservation of skeletons was noted as

G (good) = most specimens are not fragmented, corroded, or recrystallized.
M (moderate) = specimens show signs of minor fragmentation, corrosion, or recrystallization.
P (poor) = most specimens are fragmented, strongly corroded, or heavily recrystallized.

PALEOMAGNETISM

Paleomagnetic studies aboard the *JOIDES Resolution* during Leg 162 mainly comprised measurements of natural remanent magnetization (NRM) on archive halves of core sections using the cryogenic pass-through magnetometer, as well as measurements of magnetic susceptibility on whole-core sections using the multisensor track (MST). The measurement of magnetic remanence was accompanied by alternating field (AF) demagnetization in the 15–30 mT range to remove secondary magnetizations, particularly the viscous magnetization imposed by the drill string.

Magnetic Remanence Measurements

During Leg 162, the paleomagnetic laboratory on the *JOIDES Resolution* had two magnetometers for measurement of magnetic remanence: a pass-through cryogenic superconducting rock magnetometer (SRM) manufactured by 2-G Enterprises (Model 760R) and a Molspin spinner magnetometer. The laboratory has an AF demagnetizer (Model GSD-1 by the Schonstedt Instrument Co.) capable of demagnetizing discrete specimens to 100 mT. In addition, there is an in-line AF demagnetizer included in the pass-through SRM track with a coil system capable of AF demagnetization to 30 mT. The coils are enclosed in a mu-metal shield which attenuates the ambient field to less than 200 nT. The field within the AF demagnetization coils varies, particularly when the ship changes course. The shields were continually AF demagnetized in order to keep the field in the demagnetizer below 100–200 nT.

The sensing coils in the SRM measure the signal over about a 20-cm interval, and the coils for each axis have slightly different response curves. The widths of the sensing regions correspond to about 200–300 cm^3 volume of cored material. The large volume of core material within the sensing region permits accurate determination of the remanence for weakly magnetized samples, despite the relatively high background noise related to the motion of the ship.

The core-handling boat had a measurable remanence after cleansing with isopropanol, which was unremovable but very stable after AF demagnetizing to 30 mT. Subtracting the stable boat remanence from each core section measurement yielded a nominal noise level of ~10^{-5} A/m, which is 100–1000 times less intense than magnetizations measured in sediments from the North Atlantic. This nominal noise level was significantly degraded by the tendency of the cryogenic magnetometer to record false "flux jumps." Several remeasurements of core sections were sometimes necessary during these episodes of spurious flux jumps in order to keep instrumental "drift" below 10% of the core magnetization. The tendency for flux jumping can be diminished by turning off the fast slew rate option on the magnetometer electronics; however, as the computer program automatically sets the fast slew rate, the option must be exercised after the onset of remanence measurement. The pass-through SRM and its AF demagnetizer are controlled by the Quick BASIC program CRYOSECT running on a PC-AT-compatible computer.

The Molspin fluxgate magnetometer was used to carry out stepwise AF demagnetization of discrete samples. Discrete samples in soft sediment were taken using oriented standard plastic boxes (6 cm^3). The progressive AF demagnetization of discrete "pilot" samples (in the GSD-1 AF demagnetizer) was the basis for the choice of the optimal demagnetization fields in the pass-through cryogenic magnetometer. Demagnetization fields in the 10–30 mT range were required to eliminate the steeply inclined viscous magnetization imposed by the drill string. In the top 50–75 cm of many cores, a steep (drill-string) remagnetization was evident, possibly related to subtle top core deformation, which could not be removed at peak alternating fields of 30 mT. The inclination records presented in this volume have been "filtered" by eliminating those parts of the record affected by core deformation or the ubiquitous top core effect. At the base of the APC sections and within the XCB and RCB sections, core deformation and "biscuiting" of the sediment severely compromised the magnetic remanence record. Remanence measurements generally were incoherent in cores acquired by XCB/RCB drilling. On the pass-through magnetometer data, it was noted that the mud between the biscuits was often more strongly magnetized than the biscuits themselves. This may be attributed by winnowing of low density grains by circulating drill water, and concentration in the mud of heavy minerals (including magnetite).

Magnetic inclination records after AF demagnetization in the 15–30 mT range are the basis for the magnetic polarity stratigraphy. The polarity records were then matched to the geomagnetic polarity time scale. We adopt the polarity chron nomenclature from Cande and Kent (1992). Polarity chron age assignments are from Shackleton et al. (1990), Hilgen (1991a, 1991b), Cande and Kent (1995), and Berggren et al. (1995).

Magnetic Susceptibility Measurements

The magnetic susceptibility of whole-core sections was measured with a Bartington Instruments magnetic susceptibility meter (Model MS1, adapted with a MS1/CX 80-mm whole-core sensor loop set at 0.465 kHz), mounted with the gamma-ray attenuation porosity evaluation (GRAPE), *P*-wave logger, and natural gamma-ray sensor on the multisensor track (MST) (see "Physical Properties" section, this chapter). For the susceptibility measurement, the full width of the impulse response peak at half maximum is less than 5 cm. The susceptibility of discrete specimens can be measured on board with a sensor unit (type MS1B) attached to the Bartington susceptibility meter and a Kappabridge KLY-2 (made by Geofyzika Brno).

Whole-core susceptibility measurements are relatively rapid to make, are nondestructive, and provide an indication of the amount of magnetizable material in the sediment, including ferrimagnetic and paramagnetic constituents. Whole-core volume magnetic susceptibility from the MST track was measured at the low sensitivity range (1.0) of the Bartington (MS1) meter and in the SI mode, sampling every 3 cm. The SI unit of volume susceptibility (equal to J_i/H) is dimensionless as both the volume magnetization (J_i) and magnetic field strength (H) can be expressed as A/m in SI units. The susceptibility response is a function of the mineralogy as well as the shape and volume of the magnetic particles within the rocks. Magnetite and the magnetic iron sulfides (pyrrhotite and greigite) have magnetic susceptibilities several orders of magnitude greater than other iron oxide minerals (such as hematite), iron oxyhydroxides (such as goethite), or paramagnetic minerals (such as pyrite and some clay minerals). In the presence of magnetite, and in the absence of substantial concentrations of greigite and/or pyrrhotite, the susceptibility record will be primarily controlled by the concentration of magnetite.

Core Orientation

Core orientation of the advanced hydraulic piston cores (APC) was carried out using the Tensor multishot tool which is rigidly mounted onto a nonmagnetic sinker bar. At the bottom of the hole the core barrel was allowed to rest for sufficient time (2–8 min) to permit an accurate reading of the magnetic and gravity sensors. The Tensor tool consists of three mutually perpendicular magnetic sensors and two perpendicular gravity sensors. The information from both sets of sensors allows the azimuth and dip of the hole to be measured as well as the azimuth of the double orientation line on the APC core liner. Due to the high inclination of the geomagnetic field at latitudes of the Leg 162 drill sites, orientation data was judged to be of little value to the interpretation of polarity; however, it will be very important for the study of polarity transition and magnetic excursions.

Core orientation was not attempted for the first two APC cores at each hole so that the bottom-hole assembly (BHA) could first advance well into the sediment. This prevents the possibility of damage to the orientation tool due to the shock of a corer stroking out above mudline, and allows the coring to proceed quickly when the BHA is vulnerable while close to the sediment/water interface. Not all APC cores were oriented due to time constraints.

SEDIMENTATION RATES

Shipboard sedimentation rate calculations are important for preliminary paleoceanographic interpretations. In addition, post-cruise sampling plans are dependent on the initial age-depth relationships determined. On Leg 162, biostratigraphic and paleomagnetic datums were used to establish age-depth relationships. The magnetostratigraphic polarity time scale was adopted from Cande and Kent (1995) and Berggren et al. (1995). Paleomagnetic reversals were determined by pass-through cryogenic magnetometer (see "Paleomagnetism" section).

Fossil groups used for biostratigraphy included benthic and planktonic foraminifers, calcareous nannofossils, diatoms, and siliceous flagellates (see "Biostratigraphy" section). The time scale for biostratigraphic age determinations was taken from Cande and Kent (1995) and Berggren et al. (1995). At each site, paleomagnetic and biostratigraphic datums were tabulated and age-depth plots were made. Linear interpolation between reliable datums was used to calculate sedimentation rates for each site on both the meters below seafloor (mbsf) and meters composite depth (mcd) scales.

ORGANIC GEOCHEMISTRY

The shipboard organic geochemistry program for Leg 162 includes (1) real-time monitoring of volatile hydrocarbon gases, (2) measurement of the inorganic carbon concentration to determine the amount of carbonate in the sediments, (3) elemental analyses of total carbon, total nitrogen, and total sulfur, and (4) characterization of organic matter. All methods and instruments used during Leg 162 are described in detail by Emeis and Kvenvolden (1986) and in the "Explanatory Notes" chapter of the Leg 156 *Initial Reports* volume.

Hydrocarbon Gases

For safety considerations, the concentration of methane (C_1), ethane (C_2), and propane (C_3) gases are measured in every core using a Hewlett Packard 5890 Series II gas chromatograph. Gases are extracted using standard ODP headspace-sampling techniques (Kvenvolden and McDonald, 1986). Wherever gas voids occurred, vacutainer samples were taken as well. The C_1/C_2 ratio is generally used to get quick information about the origin of the hydrocarbons; that is, to distinguish between biogenic gas and gas migrating from a deeper source of thermogenic hydrocarbons. Very high C_1/C_2 ratios indicate gas (C_1) formation by microbiological processes. On the other hand, the occurrence of major amounts of C_2 (to C_5) gas at shallow depths is associated with migration of thermogenic hydrocarbon.

Inorganic Carbon

Inorganic carbon is determined using a Coulometric 5011 carbon dioxide coulometer. Approximately 10 mg of freeze-dried, ground, and weighed sediment is used for each measurement. Percentage of carbonate is calculated from the inorganic carbon (IC) content, assuming that all carbonate occurs as calcium carbonate as follows:

$$CaCO_3 = IC \times 8.33.$$

Elemental Analyses

Total carbon, nitrogen, and sulfur contents of the sediment samples are determined using a Carlo Erba Model NA1500 CHNS analyzer. Total organic carbon (TOC) content is calculated by difference between total carbon (TC) and inorganic carbon (IC):

$$TOC = TC - IC.$$

Organic Matter Characterization and Determination of Maturity

The origin of the organic matter in the sediments can be characterized using organic carbon/nitrogen (C/N) ratios. The average C/N ratio of marine zoo- and phytoplankton is between 5 and 8, whereas higher land plants have ratios between 20 and 200 (Bordowskiy, 1965; Emerson and Hedges, 1988). Organic matter type, thermal maturity, and hydrocarbon-producing (S_1, S_2, S_3, and S_4) potential are assessed using a Delsi-Nermag Rock-Eval II pyrolysis system. For details of operation, see the "Explanatory Notes" chapter of the Leg 156 *Initial Reports* volume.

INORGANIC GEOCHEMISTRY

Shipboard interstitial water analyses were performed on 5- to 15-cm whole-round sections that were cut immediately after the core arrived on deck. At all sites, samples were usually taken from the bottom of Section 4 in each of the first three cores, and in every third core thereafter. At Sites 981 and 984, suites of high-resolution interstitial water samples were obtained by cutting 5-cm-long whole-round segments from the bottom of each section (except Section 7) for the first 100 m of core. Interstitial waters were collected by applying pressure to the sediment using a titanium and stainless steel squeezer and collecting the water (modified from Manheim and Sayles, 1974). Before squeezing, the surfaces of the whole-round segment were scraped with a spatula to remove potentially contaminated exteriors. The whole-round was then placed in the squeezer atop a Whatman No. 1 filter, and pore waters were expressed by applying loads up to 40,000 lb (pressures of approximately 4150 psi) using a hydraulic laboratory press. Interstitial water samples were collected into 50-mL plastic syringes attached to the bottom of the assembly. Extruded waters were then passed through a 0.45-µm Gelman polysulfone disposable filter. Shipboard samples were stored in plastic vials pending analysis. Aliquots for future shore-based analyses were placed in glass ampules and heat sealed.

Interstitial waters were routinely analyzed for salinity with a Goldberg optical hand-held refractometer (Reichart). Salinity is reported as a unitless quantity as described by Gieskes et al. (1991). Alkalinity and pH were measured immediately after squeezing by Gran titration with a Metrohm autotitrator and Brinkmann pH electrode, respectively. Chloride was measured by titration with a precision of 0.2% and sodium was estimated by charge balance where total cation charge = total anion charge. For most analyses, the International Association of Physical Sciences Organizations (IAPSO) seawater was used for standardization.

Sodium, potassium, magnesium, calcium, chloride, and sulfate were measured by ion chromatography on 1/200 diluted aliquots in nanopure water using a Dionex DX-100. In general, the results obtained from this technique for some elements are less accurate than alternate methods including titration for Cl and charge balance calculations for Na. However, the relative trends are usually similar and can serve as a second check of results generated by the other methods. The precision of results measured by ion chromatography was generally within 2%–3%.

Silica, ammonia, and phosphate were determined by spectrophotometric methods using a Milton Roy Spectronic spectrophotometer with sample introduction by Mister Sipper.® The chemical methods employed follow those of Gieskes et al. (1991).

Strontium and lithium were determined using a Varian Spectra AA-20 atomic absorption spectrophotometer. Standards were matched in matrix composition to the samples. Lithium standards and samples were determined on 1/5 diluted aliquots in nanopure water and strontium standard concentrations were determined on 1/10 diluted aliquots. Lithium was determined by emission using an air-acetylene flame, and strontium by atomic absorption using a nitrous oxide-acetylene flame with lanthanum chloride as an ionization suppressant. The precision of these techniques is approximately <1%–2% for lithium and <4% for strontium.

PHYSICAL PROPERTIES

The purpose of physical properties measurements was threefold: (1) to provide near-continuous records for hole-to-hole correlation and construct complete stratigraphic sequences, and core-to-downhole log ties; (2) to provide estimates of properties related to composition and consolidation history of the sediments, such as porosity, natural gamma radiation, magnetic susceptibility, and shear strength; and (3) to furnish data for the calculation of synthetic seismograms, such as *P*-wave velocity and bulk density, and for the calculation of local heat flow (i.e., thermal conductivity and downhole temperatures).

The first measurement station was the multisensor track (MST), which combines four sensors on an automated track to measure bulk density, magnetic susceptibility, natural gamma-ray emission, and *P*-wave velocity on whole-core sections. Next, thermal conductivity was measured on whole-core sections in intervals where downhole temperature measurements were taken. Then the cores were split and the working half was used for further physical properties measurements. These included water content, grain density (to calculate bulk density, porosity, and related index properties), P-wave velocity, and shear strength measurements. The methods used to calculate these properties are described in the following sections.

Index Properties

Index properties, as defined for ODP shipboard procedures, include gravimetric determinations of water content, bulk density, grain (solid) density, and related properties such as porosity, void ratio, and dry density. The measured parameters are initial wet bulk mass, M_b, and dry mass and volume, M_d and V_d, respectively, after drying the samples in a convection oven for 24 hr at temperatures varying from 95°C to 105°C (Method C). Optionally, bulk volume, V_b, can be measured by gas pycnometry as well (Method B). This was done at the first two sites but was discontinued due to the questionable quality of such measurements, the extremely high rate of core recovery, and the lack of adequate numbers of beakers on board. All calculations, including the salt correction, which corrects for the phase transition of pore-water salt during drying, were performed by the shipboard IP/4D program and are summarized below (the program code is appended to the shipboard laboratory manual for index properties).

First, salt corrections on M_d and V_d are performed using the evaporated mass of pure water, M_w, a salinity $s = 0.035$, corresponding pore-water density of $\rho_{pw} = 1.024$ g/cm^3, and salt density of $\rho_{salt} = 2.257$ g/cm^3. Mass of salt is

$$M_{salt} = s/(1 - s) \cdot M_w, \tag{1}$$

and it follows that corrected pore-water mass, M_{pw}, pore-water volume, V_{pw}, solid mass, M_s, and solid volume, V_s, are, respectively:

$$M_{pw} = M_w + M_{salt} = M_w/(1 - s), \tag{2}$$

$$V_{pw} = M_{pw}/\rho_{pw}, \tag{3}$$

$$M_s = M_d - M_{salt}, \text{ and} \tag{4}$$

$$V_s = V_d - V_{salt} = V_d - M_{salt}/\rho_{salt}. \tag{5}$$

Water content, W, can be expressed as a ratio of pore-water mass, M_{pw}, to solid mass, M_s, or to bulk mass, M_b, respectively (see also ASTM Standard D 2216–80; ASTM, 1980):

$$W_s = M_{pw}/M_s = (M_b - M_d)/(M_d - sM_b), \text{ or} \tag{6}$$

$$W_b = M_{pw}/M_b = (M_b - M_d)/[(1 - s)M_b]. \tag{7}$$

Water content is often referred to as "% dry mass of sample" or "% wet mass of sample," which are $W_s \cdot 100\%$ and $W_b \cdot 100\%$, respectively. Grain (solid) density, ρ_s, and bulk density, ρ_b, were then calculated, respectively, as

$$\rho_s = M_s/V_s, \text{ and} \tag{8}$$

$$\rho_b = (M_s + M_{pw})/(V_s + V_{pw}). \tag{9}$$

Porosity (Φ) and void ratio (e) are volumetric, relative expressions of water content, assuming that all original sediment voids are represented by pore water in the recovered cores. (Note that gas which is free or in solution in situ escapes partly during core recovery, and almost completely disappears from the voids when the cores are sectioned and split; therefore, gas is not quantified by gravimetric methods which assume water saturation). Porosity and void ratio are calculated, respectively, as

$$\Phi = V_v/V_b = \rho_b/\rho_{pw} \cdot W_b, \text{ and} \tag{10}$$

$$e = V_v/V_s = \rho_s \cdot W_s/\rho_{pw}. \tag{11}$$

Dry density is used to estimate the mass accumulation rate for a given depth interval and is defined as

$$\rho_d = M_s/V_b = \rho_b/W_s \cdot W_b. \tag{12}$$

Samples for index properties measurements were taken at frequency of one to two per core section. However, where frequent lithological changes occurred, denser sampling was undertaken to ensure measurements from all significant lithologies throughout the core. Discrepancies from this are described in individual site chapters.

The samples for index properties measurements were taken within 5 cm of the position for measurements of undrained shear strength and P-wave velocity (see below). This ensured that the different parameters represent the same sediment type, and can be correlated without interpolation. In XCB and RCB cores, which frequently showed "biscuiting" type of disturbance, particular care was taken to sample undisturbed parts of the core sections and to avoid the drilling slurry.

Mass determinations were precise to within ±0.005 g (<0.5%) and volume determination to within ±0.02 cm^3 (<1%). Balance and pycnometer precision are estimated from control measurements run routinely on a mass standard and a calibration sphere of known volume. Calibrations were performed when the values deteriorated. The total standard error for index properties is estimated to be less than 2%. This precision estimate is unrelated to potential deviations from in situ values.

Bulk Density (Gamma-ray Attenuation)

An additional estimate of bulk density has been obtained from continuous logging of whole-round core sections with the "gamma-ray attenuation porosity evaluator" (GRAPE). This device measures the electron density, ρ_e, which is related logarithmically to the gamma-ray attenuation by

$$\rho_e = 1/\mu d \cdot \ln(N_0/N), \tag{13}$$

where μ is the gamma-ray attenuation coefficient, d the thickness of the sample (maximum core diameter), N_0 the incident gamma-ray intensity and N the detected gamma-ray intensity after attenuation. For a certain range of electron energies caused largely by Compton scattering (about 0.2–2.0 MeV), the electron density is related to the bulk density, ρ_b, by

$$\rho_e = \rho_b(Z/A)N_A, \tag{14}$$

where Z is the atomic number, A the atomic mass, and N_A is Avogadro's number. Because Z/A is about 0.5 for all common minerals, the bulk density of minerals can be accurately measured from the gamma-ray intensity ratio, N_0/N, using a calibration based on aluminum standards of different thicknesses. Z/A is about 1 for water, however, and a correction based on a porosity evaluation is therefore applied to the first approximation of ρ_b (reported as

"GRAPE density") to get a more realistic "corrected GRAPE density" (Boyce, 1976).

The Leg 162 GRAPE densities were all systematically too low by about 10% (0.2 to 0.4 g/cm^3) when compared to gravimetric data and downhole logging data. This was also apparent when comparing the Hole 907B and 907C data with the records from Hole 907A, which was drilled during Leg 151 when this problem was not present. It appears that the systematic underestimation of GRAPE densities has occurred for several legs, perhaps starting with Leg 155 after a new power supply was installed. We considered the following potential sources of this problem: (1) gamma-ray source and sensor were not properly aligned; (2) the power supply was operating at 0.92 kV, which appears to be lower than the recommended voltage; this could result in a biased amplification of the electron energy spectrum; (3) the detector threshold was set so as to measure low electron energy events (<150 keV) which are sensitive to lithology (photoelectric effect), rather than measure the higher energy events which are only sensitive to bulk density (Compton scattering); (4) geometric discrepancy between calibration runs and core section runs could make calibrations invalid; (5) an unknown change has occurred in the calculation program. After running many calibrations and control measurements, we were unable to explain certain discrepancies between MST-generated and manually calculated calibration coefficients, which may be an unrelated problem since it cannot account for the magnitude of the general density offset. Because of the all-time record core recovery rate during the first five weeks of the cruise we could not seriously attempt to study this problem in further detail. The data were consistent and useful for core-to-core correlation. They can be linearly corrected for the offset. During the port call following Leg 162, it was confirmed that the source-sensor system had not been properly aligned. An entirely new MST program was installed at that time so that the Leg 163 and subsequent data could not be tested for the flaw observed on Leg 162.

GRAPE density was sampled at 2-second intervals, regardless of whether the core was moving. This led to variable sample intervals ranging from a minimum (width of gamma-ray beam, or about 0.4 cm) while the core was stopping for other measurements, to the maximum distance traveled in 2 s while the core was in motion (2 cm). Two to three and six GRAPE measurements were accumulated at measurement depths where the core was stopping for magnetic susceptibility and natural gamma-ray measurements, respectively.

Natural Gamma-ray Emission

Natural gamma-ray measurements were taken for periods of 10 s every 10 cm while the core was stopped. No calibration was performed at the beginning of the leg. Background radiation was determined with a water core to be about 9 cps at the beginning of the leg. This has been the background radiation within ±1 cps over the past two years. The total counts were useful for composite depth construction and definition of some lithologic trends. The relatively short sampling period of 10 s did not allow for accumulation of sufficient counts to evaluate the spectrum of five energy windows acquired routinely by the MST program.

Magnetic Susceptibility

Magnetic susceptibility was measured with the Bartington meter MS1 using a 8-cm loop and the low sensitivity setting 1.0. Sample periods were 3 s and sample intervals 3 cm. Magnetic susceptibility was the single most useful record for core-to-core correlation and composite depth construction.

Velocity

P-wave velocity was measured continuously on whole-round core sections, orthogonal to the core axis, with the *P*-wave logger (PWL) mounted on the MST. In addition, *P*-wave velocity was measured on split-core sections using two types of transducer pairs in the digital sound velocimeter (DSV), T1 and T2, which were inserted along and orthogonal to the core axis, respectively, into soft sediment, and T3 (modified Hamilton frame velocimeter), which measured orthogonally across the split-core section and core liner through transducer contact with the sediment on top and the core liner on bottom, respectively. Use of the T1 and T2 transducers was stopped when the sediment started to crack during insertion of the transducers, commonly below 30–50 mbsf. In well-compacted or indurated sediments, T3 was also used on discrete samples, with transducer contact with the sediment both on the top and bottom. Split-core velocity measurements were made at intervals similar to those used in measuring the index properties (see above) and shear strength (see below).

Measurement directions are in accordance with ODP standards (i.e., z is parallel to the core axis and x and y are orthogonal to the core axis (Fig. 8). When measuring in the z-direction with T1, the transducer distance is 7 cm, whereas measurements in the x and y directions with T3 and T2, respectively, affect approximately a 2-cm interval of the core. The tables in individual site chapters give the midpoints of the measured intervals which correspond to the calculated depths (mbsf) used for plotting the data.

The PWL requires two types of calibrations which were performed at the beginning of the leg. First, a two-point calibration was carried out for the displacement transducer using a standard core liner and a block standard. The displacement transducer measures the core thickness and uses this measure to calculate *P*-wave velocity in the sediments. Secondly, a 1-point velocity calibration was done: the water standard was run and a correction factor compensating for velocity in the liner and electronic delay was adjusted to give the expected theoretical velocity in water at laboratory temperature.

The T1 and T2 split-core velocimeter calculates velocity based on a fixed distance measured with a caliper, a delay constant determined with a water standard, and measured traveltime. The T3 system calculates velocity from the distance determined by a digital scale and measured traveltime.

Undrained Shear Strength

Measurements of undrained shear strength (S_u) were taken at intervals similar to those of velocity and index properties measurements (see above).

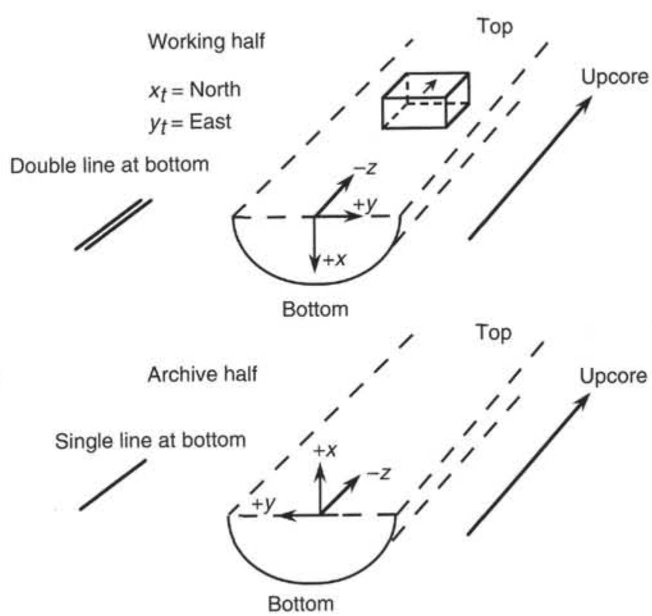

Figure 8. Core orientation conventions for split-core sections and discrete samples.

Motorized Vane Shear Device

Undrained shear strength (S_u) was determined using the ODP motorized miniature vane shear apparatus and following the ASTM D 4648-87 procedure (ASTM, 1987). A four-bladed vane was inserted into the split-core and rotated at a constant rate of 90°/min to determine the torque required to cause a cylindrical surface (approximately 1 cm in diameter) to be sheared by the vane. The difference in rotational strain between the top and bottom of a linear spring was measured using digital shaft encoders. A measured strain-calculated torque plot was displayed by the data acquisition program, and maximum spring deflection at peak strength was determined by the program and could easily be verified or adjusted by the user.

The vane blade constant, k, is calculated as

$$k = 2/\pi \cdot D^2 \cdot H/(1 + D/3H), \qquad (15)$$

where D and H are the vane diameter and height in m, respectively, and k has the units of m^{-3}. Torque, T (Nm), is calculated from the measured spring deflection, Δ, and the spring calibration constant, b, as follows:

$$T = b \cdot \Delta. \qquad (16)$$

Four springs were used with the following constants (Nm/°): #1 = 0.0092109, #2 = 0.018857, #3 = 0.030852, and #4 = 0.045146.

Spring calibrations are contracted out by ODP and are not performed on the ship. The undrained shear strength was then calculated by

$$S_u = T/K. \qquad (17)$$

The main sources of error using the motorized vane shear device are sand- and gravel-sized particles in the sediments and fracturing of the sediment during the test. The latter was particularly a problem when S_u exceeded 100–150 kPa. It should be borne in mind that the relationship between strength measurements on unconfined core material can only be related to in situ properties by empirical relationships that are dependent on the sediment and other characteristics of the sedimentary environment.

Pocket Penetrometer

A pocket penetrometer was used when the sediment was neither too soft nor too brittle. The penetrometer is a flat-footed, cylindrical probe 0.5 cm in diameter that is pushed 6.4 mm deep into the split-core surface. The resulting resistance is the unconfined compressive strength, or $2S_u$. The mechanical scale is in units of kg/cm^2, which are converted into units of kPa by

$$2S_u\,(\text{kPa}) = 2S_u\,(\text{kg/cm}^2) \cdot 98.1\,(\text{kPa/[kg/cm}^2]). \qquad (18)$$

The maximum S_u that can be measured with the pocket penetrometer is 220 kPa.

Fall-cone Penetrometer Device

At Sites 986 and 987, undrained shear strength was also measured by means of a fall-cone device (Skempton and Bishop, 1950), provided for Leg 162 by one of the shipboard scientists. The fall-cone device provides a rapid and simple method for determination of undrained shear strength for undisturbed (as well as remolded) clays. A cone of known weight and apex angle is lowered to touch the sediment surface. After release it penetrates into the sediment only by its own weight. Based on empirical relationships, the penetration in millimeters can be directly converted to undrained shear strength in kPa. Four different cones were used: 10g/30°, 60g/60°, 100g/30°, and 400g/30°, covering the shear strength intervals of 0.1–1.5 kPa, 1.1–9.0 kPa, 7.0–39 kPa, and 17.5–245.0 kPa, respectively.

Fall-cone measurements affect a smaller volume of sediment during the measurement, and are therefore less affected by sand- and gravel-sized material than are vane shear measurements. Fracturing of the sediment, which is a main cause of error in the vane shear measurements, is also avoided using the fall-cone device. Furthermore, the fall-cone device has been used in many earlier studies of glacial sediments around Svalbard; thus, values of undrained shear strength obtained during Leg 162 can be better compared with results of previous studies in this region.

Heat Flow

Heat flow was determined at several sites using thermal conductivity measurements on whole-round core sections, and downhole temperature measurements using the Adara (manufacturer's name) temperature probe which fits into the coring shoe of the advanced piston core (APC) barrel.

Thermal Conductivity

Thermal conductivity was measured using needle probes in full-space configuration. At the beginning of the leg, the instrument was calibrated to produce the heat in the needle specified in the shipboard TC/PC program which is used to calculate thermal conductivity. In addition, three standard materials, macor (1.61 ± 0.1 W/[m·K]), red rubber (0.96 ± 0.1 W/[m·K]), and black rubber (0.54 ± 0.05 W/[m·K]), were measured with the five needles used for core measurements. Average values for each standard were used to calculate regression coefficients (Table 3), which were entered into the program and used for linear corrections in thermal conductivity calculations.

The data acquisition program performed a temperature drift study for each run, and measurements were carried out when the cores had equilibrated to ambient temperature (about 3–4 hr after recovery). While the needle was heated, the temperature T was measured with elapsed time t and related to the thermal conductivity of the sediment by

$$T = (q/4\pi k)\ln(t) + C, \qquad (19)$$

where q is the heat input per unit time and unit length (W/m^2), and k is the thermal conductivity (W/[m·K]). The term C includes temperature drift during measurement as well as nonlinearity resulting from imperfections in the experiment. The equation is solved for k by the program using least-squares method. An interactive display allows the user to determine the time interval used in the fit. The interval was generally set between 60 and 240 s.

At Sites 981 and 984, where we conducted a relatively extensive heat-flow program, an additional correction was applied to normalize thermal conductivity data for needle-probe bias. Control measurements performed on the red rubber standard were averaged for each needle probe used at each site. The mean of the needle averages was used as the normal value for red rubber, and all data were normalized to that value by a factor M_{rr}/M_n, where M_{rr} is the normal value for red rubber and M_n is the mean value for the needle probe used (Table 4).

Thermal conductivities collected on more than one hole at a site were combined into one data set using the meters composite depth scale (mcd; see "Composite Depths" section, this chapter). Using the mcd scale greatly improved the accuracy of the data splice as compared to simply using the mbsf scale for all data. After the data were combined, depths were scaled to a corrected meters composite depth (cmcd) to ensure that thermal conductivity values measured in the expanded cores matched the depths of the downhole temperature mea-

Table 3. Thermal conductivity standard measurements and regression coefficients used to correct raw measurements.

Sites 981 and 984:				
Accepted measurements				
Black rubber	0.54 ± 0.02 W/(m·K)			
Red rubber	0.96 ± 0.05 W/(m·K)			
Macor	1.61 ± 0.08 W/(m·K)			
Standard	Average measurement (W/[m·K])	Std. dev.	Slope	Intercept
Needle 352				
Black rubber	0.551	0.033		
Red rubber	0.908	0.024		
Macor	1.872	0.074	0.782	0.169
Needle 353				
Black rubber	0.561	0.015		
Red rubber	0.926	0.018		
Macor	1.980	0.019	0.724	0.200
Needle 354				
Black rubber	0.585	0.058		
Red rubber	0.924	0.029		
Macor	2.050	0.113	0.692	0.216
Needle 360				
Black rubber	0.491	0.010		
Red rubber	0.936	0.058		
Macor	1.728	0.049	0.860	0.132
Needle 361				
Black rubber	0.503	0.062		
Red rubber	0.909	0.046		
Macor	1.761	0.053	0.837	0.152
Sites 986 and 987:				
Accepted measurements				
Black rubber	0.54 ± 0.02 W/(m·K)			
Jello	0.678 ± 0.014 W/(m·K)			
Macor	1.75 ± 0.08 W/(m·K)			
Standard	Average measurement (W/[m·K])	Std. dev.	Slope	Intercept
Needle 352				
Black rubber	0.535	0.012		
Jello	0.702	0.011		
Macor	1.764	0.070	0.990	0.003
Needle 353				
Black rubber	0.544	0.009		
Jello	0.711	0.010		
Macor	1.925	0.075	0.872	0.074
Needle 354				
Black rubber	0.537	0.162		
Jello	0.696	0.009		
Macor	1.794	0.011	0.967	0.015
Needle 360				
Black rubber	0.545	0.009		
Jello	0.643	0.014		
Macor	1.814	0.052	0.937	0.054
Needle 361				
Black rubber	0.537	0.019		
Jello	0.659	0.010		
Macor	1.720	0.091	1.018	0.002

surements. This was done on a core-by-core basis by adjusting curated sample depth below top of core i ($cbct_{ij}$) by the ratio

$$R_i = D_i/(C_i + \Delta x_{(i+1)}), \tag{20}$$

where D_i and C_i are the drilled interval and curated length for core i, respectively, and $\Delta x_{(i+1)}$ is the offset given in the composite depth table for the subsequent core i + 1, representing the coring gap between core i and core i + 1. Corrected sample depths below core top ($xbct_{ij}$) are then

$$xbct_{ij} = R_i \cdot cbct_{ij} \tag{21}$$

and are added to the drilling datum for the top of core i in meters below seafloor ($mbsf_i$) to derive sample depth below seafloor at the corrected meters composite depth scale (cmcd):

$$cmcd = mbsf_i + xbct_{ij}. \tag{22}$$

Downhole Temperature

Downhole temperature measurements followed the procedures and used the tools described by Fisher and Becker (1993). Tool 12 was generally used. Tool 18 was used in addition to Tool 12 when measurements were taken on subsequent cores over certain intervals in Holes 981C and 984B. Tool 12 was damaged during an attempted deployment in Hole 984D.

Bottom-water temperatures were measured during several runs by holding the tool 20 m above mudline for about 10 min before and after coring. The bottom water curves, usually expected to be flat, showed an equilibration pattern similar to the sediment measurements. Equilibrium temperatures were calculated using the TFIT processing program and a thermal conductivity of 0.68 W/(m·K) for water. In addition, we measured bottom water on "dedicated runs," before the hole was spudded at Sites 984, 986, and 987, without taking a subsequent sediment measurement for operational reasons. Given the possibility that bottom-water temperature measurements are influenced by warm water from the borehole, it appears to be more accurate to take one dedicated measurement before the hole is spudded.

Geotechnical Stratigraphy

A geotechnical stratigraphy was established at each site based on trends in the physical properties. Data from downhole logging were also used in the definition of geotechnical units where core recovery was inadequate to provide a representative section through the drilled depth. The criteria used to define the geotechnical stratigraphy were as follows: Geotechnical units were defined from the total character of a portion of the sedimentary section, for example, high or low val-

Table 4. Thermal conductivity standard (red rubber) measurements taken every run and used to normalize data for needle bias.

	Probe 353	Probe 354	Probe 358	Probe 360	Probe 361	Average of needle means
Sites 980/981						
n (measured)	14	13	14	16	15	
n (not used)	1	0	1	1	0	
Mean (W/[m·K])	0.890	0.876	0.881	0.957	0.903	0.901
Std. dev.	0.039	0.038	0.018	0.032	0.019	
Site 984						
n (measured)	7	6	8	8	9	
n (not used)	1	0	0	1	1	
Mean (W/[m·K])	0.911	0.864	0.881	0.944	0.903	0.901
Std. dev.	0.033	0.021	0.022	0.019	0.038	

ues, frequent small-scale variations, or steadily increasing or decreasing values with depth. Geotechnical subunits were defined within units, typically based on changes in gradients of measured values, or shorter intervals of different character from that typical for the unit, for example, a short low within a general high. Definition of unit and subunit boundaries were always based on more than one parameter.

WIRELINE LOGGING

The Borehole Research Group of Lamont-Doherty Earth Observatory (LDEO-BRG), in conjunction with Schlumberger Well Logging Services, provided the geophysical well logging aboard the *JOIDES Resolution.* Primarily designed for use in hydrocarbon exploration, logging tools have been adapted to meet ODP requirements and hole conditions. This includes the reduction of tool diameter to allow insertion into the 3.8-inch drill-string bore.

Downhole logs are used to determine the geophysical, chemical, and structural properties of formations penetrated by drilling. When core recovery is incomplete, log data serve as a proxy for physical properties and sedimentological data and permits the core to be placed in its proper stratigraphic position within the cored interval. Logs also complement discrete core measurements and offer the additional advantage over core-based analyses in that they are rapidly collected and represent continuous in situ measurements. Geophysical well-logging is also used to aid in characterization of sedimentary sequences when integrated with core and seismic reflection data.

During Leg 162, we used the Quad combination, the Formation MicroScanner (FMS), the Geological High-Sensitivity Magnetic Tool (GHMT-A), and Geochemical Logging Tool (GLT) strings. All tools used during Leg 162 were run at the highest resolution possible to provide detailed information for the paleoclimate research objectives of this leg (Table 5).

Well-Logging Operations

After coring was completed, the holes were flushed of sediment fill by circulating heavy viscous drilling fluid or seawater through the drill pipe to the mudline. The drilling assembly was then pulled up to the upper logging point (~80–100 mbsf) and the pipe was run down to the bottom of the hole again to condition the borehole for the logging program. Tool strings made up of one or more combinations of sensors were then lowered downhole using a 7-conductor cable. When necessary, a wireline heave-motion compensator (WHC) was employed to minimize the effect of ship's heave on the tool position in the borehole. LDEO-BRG replaced the WHC with a new system during the port call prior to Leg 162. This new system was installed to improve the quality of downhole logs through its ability to respond faster and more accurately to the ship's heave while on site. Data collected from logs and WHC tests conducted during the leg will be used to evaluate the performance of the new system.

Logging Tool Strings

After coring was completed at a hole, a tool string (a combination of several sensors) was lowered downhole on a conductor cable, and each of the sensors continuously monitored some property of the formation or borehole. Data are typically recorded at 15-cm vertical intervals. The depths of investigation into the formation (and the vertical resolution) are sensor-dependent (Table 5).

During each logging run, incoming data were acquired by the MAXIS 500 system capable of processing data from the geophysical, magnetic, and the FMS tool strings. Data from the MAXIS 500 are generated in a special data format (Digital Log Information Standard, or DLIS). The GLT was operated by the older Cyber Service Unit (CSU) computer, which generates data in Log Information Standard

Table 5. Approximate vertical resolution of various logging tools used during Leg 162.

Tool	Vertical resolution	Depth of investigation
Phasor Dual Induction Tool (DIT)		
Deep resistivity (ILD)	200 cm, 88 cm, 59 cm	1.5 m
Medium resistivity (ILM)	150 cm, 88 cm, 59 cm	76 cm
Shallow focused (SFL)	59 cm	38 cm
Natural Gamma Tool (NGT)	46 cm 15–30 cm	Variable
Litho-Density Tool (HLDT)		Variable
Density, photoelectric effect	49 cm (6-in. sampling) 35 cm (2-in. sampling) 20 cm, Alpha processing 30 cm, Alpha processing (2 in.)	15–60 cm
Dipole Shear Imager (DSI)	30 cm Special processing, 15 cm	Variable 10–60 cm
Sonic Digital Tool (SDT-C/array)	30 cm Special processing, 15 cm	Variable 10–60 cm
Gamma-ray Spectroscopy Tool (GST)	15 cm 12–20 cm	Variable
Aluminum Activation Tool (AACT)	25 cm 12–20	Variable
Dual Porosity Compensated Neutron Tool (CNT-G)	55 cm (6 in. sampling) 33 cm, Alpha processing (6-in. sampling) 25.4 cm, Alpha processing (2-in. sampling)	Variable and porosity dependent (15–60 cm)
Formation MicroScanner (FMS)	5 mm	5–25 cm
Lamont Temperature Logging Tool (TLT)	(1) fast-response reading (1-s time constant)/second (2) slow-response, high-accuracy reading (10-s time constant)/10 s; *vertical resolution depends on logging speed.*	
Geological High-Sensitivity Magnetic Tool (GHMT-A)	30–50 cm	Variable

Notes: Standard sampling is at 15-cm (6 in.) intervals and high-resolution sampling is at 5.5-cm (2 in.) intervals. Alpha processing is a special high-resolution processing routine. Depth of investigation is dependent upon the formation and borehole environment; these values are only estimates. Depth resolution of final processed Geochemical Logging Tool (GLT = NGT, CNT-G, AACT, and GST) data is between 0.3 and 1 m.

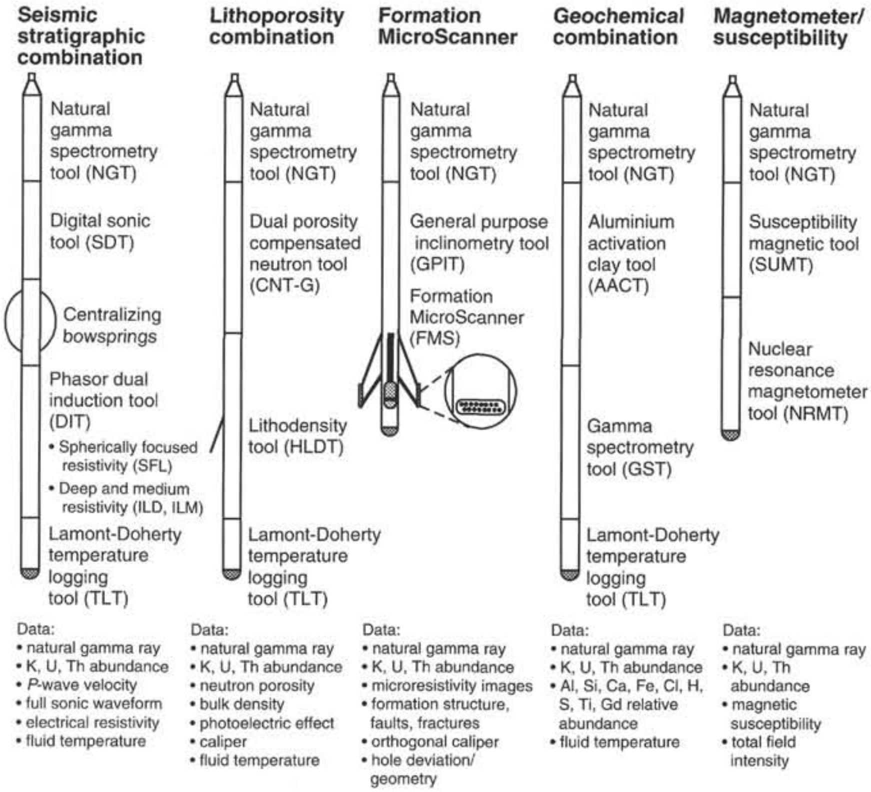

Figure 9. Schematic diagram of Schlumberger logging tool strings commonly used during ODP legs. Tool strings are not drawn to scale. See Figure 10 for details on the geochemical combination.

(LIS) format. These LIS data from the GLT are converted to DLIS format for shore-based log processing.

Individual logging tools were combined in four different strings (Fig. 9) during Leg 162: (1) the Quad combination, which consists of the seismic stratigraphic combination (NGT, LSS/SDT, DIT, and TLT) and the lithoporosity combination (NGT, CNT-G, HLDT/CALIPER, TLT), (2) the geochemical combination (NGT, AACT, GST, TLT), (3) the Formation MicroScanner (FMS) tool, and (4) the geological high-sensitivity magnetic tool string (GHMT-A) shown as "magnetometer/susceptibility" in Figure 9). The LDEO temperature logging tool (TLT) was attached, whenever possible, to the base of tool strings to obtain downhole formation/fluid temperatures. The natural gamma-ray tool (NGT) was run as part of each tool string to correlate depths between different logging runs.

Logging Tools

The specifics of the standard wireline logging tools available to ODP are described in a recent Wireline Logging Services Guide (Borehole Research Group, 1994). Information on the resolution of these tools is summarized in Table 5. A brief description of the GHMT-A tool, which is not a standard logging tool but was used during Leg 162, is provided below. In addition, the method used to produce synthetic seismograms is described in the "Underway Geophysics and Seismic Stratigraphy" section (this chapter). Further information on logging-tool principles and applications can be found in Ellis (1987), Schlumberger (1989), Timur and Toksöz (1985), Dewan (1983), and Hertzog et al. (1989)

Geological High-Sensitivity Magnetic Tool String (GHMT-A)

This tool string was developed jointly by Schlumberger and French government research institutions (CEA-LETI and CNRS-ENS). The individual tools were designed and constructed by a branch of the French Atomic Energy Commission (CEA-LETI), which also developed the analysis software.

The GHMT-A consists of a high-sensitivity total magnetic field sensor (NRMT) coupled with a magnetic susceptibility sensor (SUMT), which are used to detect borehole magnetic polarity transitions and susceptibility variations, respectively. The NRMT measures the frequency of proton precession between a calibrated applied polarizing field and the Earth's magnetic field that is proportional to the total field intensity of the Earth. An average precision of 0.5 nT is based on duplicate runs. Its sensitivity is about 10^{-2} nT. The SUMT measures mutual inductance caused by the surrounding borehole lithology using a transmitter coil and a receiver coil separated as a two-coil induction sonde. The operating frequency is about 200 Hz. The precision between duplicate runs is generally better than 3 ppm (3×10^{-6} SI), and the sensitivity of the sonde is almost 10^{-6} units. Data are recorded every 5 cm (Schlumberger, 1994).

Magnetic induction, B, in a borehole depends on position p and time t (Pozzi et al., 1988), with

$$B(p,t) = Br(p) + Ba(p) + Bf(p) + Bt(p,t),$$

where $Br(p)$ is the dipolar Earth's field and $Ba(p)$ is the anomaly field related to large-scale heterogeneities in susceptibility or in magnetic remanence. In the absence of such heterogeneities, the spatial variation of Br with depth is linear. $Bf(p)$ is the induction due to the magnetization (induced and remanent) of the sediments around the borehole, and can easily be separated from $Br(p)$ and $Ba(p)$ by subtracting the Earth's magnetic field gradient and by applying a high-pass filter. $Bt(p,t)$ is time dependent and represents the induction due to transient variations of the Earth's magnetic field. At sea, the time-dependent component can be estimated by repeat sections. To obtain direct magnetostratigraphy from $Bf(p)$, the susceptibility and the total field measurements are combined to discriminate between the induced and remanent magnetizations. Specifications of the probes, such as impulse response, calibration ratio, and geomagnetic location of the hole, are used to calculate the susceptibility effect on the scalar total field magnetometer. From these data the scalar remanent magnetization can be calculated (Pages et al., 1993).

Log Data Quality

Log data quality may be seriously degraded by rapid changes in the hole diameter and in sections where the borehole diameter is greatly increased or washed out. The result of these effects is to impair logging by causing "bridging" or "tool sticking" and to increase the fluid volume between the formation and the logging tool. Deep investigation devices such as resistivity and velocity tools are least sensitive to borehole effect. Nuclear measurements (density, neutron porosity, and both natural and induced spectral gamma ray) are more sensitive due to their shallower depth of investigation and because of the effect of increased drill-fluid volume on neutron and gamma-ray attenuation. Corrections can be applied to the original data to reduce these effects. Very large washouts, however, cannot be corrected for.

Post-Cruise Log Data Processing

Processing, quality control, and display of the logging data were performed at each of the five holes logged during Leg 162 by the Borehole Research Group (BRG) at LDEO, the Leicester University Borehole Research Group (LUBR), and the Institut Mediterraneen de Technologie, using Schlumberger "Logos" software and additional programs developed by members of the BRG. Displays of most of these processed data appear with accompanying text at the end of the appropriate site chapters in this volume. Files of all processed logs (including FMS, dipmeter, temperature data, high-resolution density and neutron data, and sonic waveforms not shown in printed form) and explanatory text are included on the CD-ROM enclosed in the back pocket of this volume; a directory of the contents of the CD-ROM is found at the front of this volume.

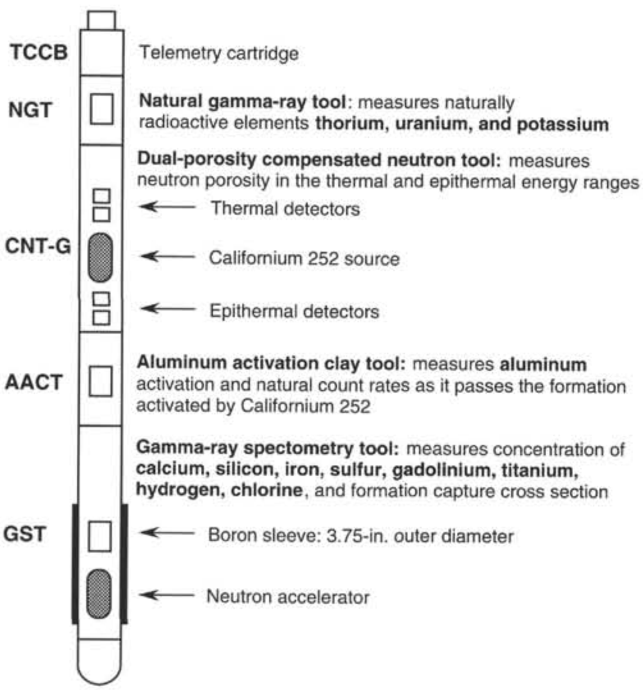

Figure 10. Schematic drawing of the Schlumberger geochemical logging tool string used in the Ocean Drilling Program.

Shore-based processing of data from each hole consisted of (1) depth adjustments of all logs to a common measurement below the seafloor, (2) corrections specific to certain tools, and (3) quality control and rejection of unrealistic values.

The depth-shifting procedure is based on an interactive, graphical depth-match program that allows the processor to visually correlate logs and define appropriate shifts. The reference log and the log to be adjusted in depth are displayed side-by-side on a screen, and vectors connect the two at positions chosen by the user. The total gamma-ray curve (SGR) from the NGT tool run on each logging string was used in most cases to correlate the logging runs. In general, the reference curve is chosen on the basis of constant, low cable tension and high cable speed (tools run at faster speeds are less likely to stick and are less susceptible to data degradation caused by ship's heave). Other factors, however, such as the length of the logged interval, presence of bottom-hole assembly, and the statistical quality of the collected data (better statistics are obtained at lower logging speeds) are also considered in the selection. A list of the amount of differential depth shifts applied at each hole is available upon request to BRG (LDEO).

Specific tool corrections were performed on the gamma-ray data to account for changes in borehole size and for the composition of the drilling fluid. Processing techniques unique to the AACT and GST tools of the geochemical string (Fig. 10) are described in detail below.

Quality control was performed by cross-correlation of all logging data. If the data processor concluded that individual log measurements represented unrealistic values, the choices were to either discard the data outright and substitute the null value of "–999.25," or identify a specific depth interval containing suspect values that must be used with caution. The latter are noted in the text that accompanies all processed log displays. Quality control of the acoustic data was based on discarding any of the four independent transit-time measurements that were negative or that fell outside a range of reasonable values selected by the processor.

In addition to the standard 15.24-cm sampling rate, bulk density and neutron data were recorded at a sampling rate of 2.54 and 5.08 cm, respectively. The enhanced bulk density curve is the result of Schlumberger enhanced processing technique performed on the MAXIS system onboard. While in normal processing short-spacing data is smoothed to match the long-spacing one, in enhanced processing this is reversed. In a situation where there is good contact between the HLDT pad and the borehole wall (low density correction) the results are improved, because the short-spacing data have better vertical resolution.

Locally, some intervals of log data appeared unreliable (usually due to poor hole conditions) and were not processed. In general, a large (>12 in.) and/or irregular borehole affects most recordings, particularly those that require eccentralization (HLDT) and a good contact with the borehole wall. Hole deviation can also degrade the data; the FMS, for example, is not designed to be run in holes that are more than 10° off the vertical, as the tool weight might cause the caliper to close.

Processing of Leg 162 Geochemical Data[3]

Geochemical Tool String

The geochemical logging tool string (GLT) consists of four separate logging tools: the natural gamma-ray spectrometry tool (NGT), the compensated neutron tool (CNT), the aluminum activation clay tool (AACT), and the gamma-ray spectrometry tool (GST). A schematic drawing of the GLT, which was run in Hole 984B on Leg 162, is shown in Figure 10. These four tools use three separate modes of gamma-ray spectroscopy for a comprehensive elemental analysis of

[3] Lee Ewart and Peter K. Harvey, Borehole Research, Department of Geology, University of Leicester, Leicester, LE1 7RH, United Kingdom.

the formation. The NGT is located at the top of the tool string so that it can measure the naturally occurring radionuclides, thorium (Th), uranium (U), and potassium (K), before the formation is irradiated by the nuclear sources contained in the lower tools. The CNT, located below the NGT, carries a californium (^{252}Cf) neutron source to activate the Al atoms in the formation. The AACT, a modified NGT, is located below the ^{252}Cf source, measuring the activated gamma rays in the formation. By combining the AACT measurement with the previous NGT measurement, the background radiation is subtracted out and a reading of formation Al is obtained (Scott and Smith, 1973). The gamma-ray spectrometry tool, at the base of the string, carries a pulsed neutron generator to induce prompt-capture gamma-ray reactions in the borehole and formation and an NaI(Tl) scintillation detector to measure the energy spectrum of gamma rays generated by the prompt neutron capture reactions. As each of the elements in the formation is characterized by a unique spectral signature, it is possible to derive the contribution (or yield) of each of the major elements silicon (Si), iron (Fe), calcium (Ca), titanium (Ti), sulfur (S), gadolinium (Gd), and potassium (K) from the measured spectrum and, in turn, to estimate the relative abundance of each in the formation when combined with the elemental concentrations from the NGT and AACT (Hertzog et al., 1989). The GST also measures the hydrogen (H) and chlorine (Cl) in the borehole and formation, although these elements are not directly used for determining the rock geochemistry.

The only major rock-forming elements not measured by the geochemical tool string are magnesium (Mg) and sodium (Na); the neutron-capture cross sections of these elements are too small relative to their typical abundances for the GLT to detect. A rough estimate of Mg+Na can be made in some instances by using the photoelectric factor (PEF), measured by the lithodensity tool (Hertzog et al., 1989). This calculation was not implemented on the geochemical data Leg 162 as the (Mg+Na) component was generally below the detection resolution of this technique (Pratson et al., 1993).

Data Reduction

The well-log data from the Schlumberger tools are transmitted digitally up a wireline and are recorded and processed on the *JOIDES Resolution* in the Schlumberger Cyber Service Unit (CSU). The results from the CSU are made available as "field logs" for initial, shipboard interpretation. Subsequent reprocessing is necessary to correct the data for the effects of fluids added to the well, logging speed, and drill-pipe interference. Processing of the spectrometry data is required to transform the relative elemental yields into oxide weight fractions.

The processing is performed with a set of log-interpretation programs written by Schlumberger but have been slightly modified to account for the lithologies and hole conditions encountered in ODP holes. The processing steps are summarized below:

Step 1: Reconstruction of relative elemental yields from recorded spectral data

This first processing step compares the measured spectra from the gamma-ray spectrometry tool with a series of "standard" spectra to determine the relative contribution (or yield) of each element. These "standards" approximate the spectrum of each element. Using a weighted, least-squares inversion method, the relative elemental yields are calculated at each depth level.

Six elemental standards (Si, Fe, Ca, S, Cl, and H) are used to produce the shipboard yields, but three additional standards (Ti, Gd, and K) can be included in the post-cruise processing to improve the fit of the spectral standards to the measured spectra (Grau and Schweitzer, 1989). The ability to detect an element is principally dependent on the size of its capture cross section and its abundance in the formation. Although Ti, Gd, and K often appear in the formation in very low concentrations, they can make a significant contribution to the measured spectra because they have large neutron-capture cross sections. Gd, for example, has a capture cross section of 49,000 barns, whereas that of Si is 0.16 barns (Hertzog et al., 1989). Therefore, including Gd is necessary when calculating the best fit of the standard spectra to the measured spectrum, even though it typical concentration is only a few ppm.

The elemental standards (Si, Ca, Fe, Ti, Gd, Cl, and H) were used in the spectral analysis step for Hole 984B. The spectral standards for S and K were not used in the final analysis because their inclusion in the spectral inversion was found to increase the noise level in the other elemental yields A linear 10-point (5 ft, 1.52 m) moving average was applied to the output elemental yields to increase the signal to noise ratios.

Step 2: Depth-shifting

Geochemical processing involves the integration of data from the different tool strings; consequently, it is important that all the data are depth-correlated to one reference logging run. The NGT, run on each of the logging tool strings, provides a spectral gamma-ray curve with which to correlate each of the logging runs. A reference run is chosen on the bases of constant and low cable tension, and high cable speed (tools run at faster speeds are less likely to stick and are less susceptible to data degradation caused by ship's heave). The depth-shifting procedure involves picking a number of reference points based on similar log character and then invoking a program which expands and compresses the matching logging run to fit the reference logging run. The main run of the geochemical logging tool string was chosen as the reference run for Hole 984B on Leg 162.

Step 3: Calculation of total radioactivity and Th, U, and K concentrations

The third processing routine calculates the total natural gamma-ray radiation in the formation, as well as concentrations of Th, U, and K, using the counts in five spectral windows from the NGT (Lock and Hoyer, 1971). This routine resembles shipboard processing; however, the results are improved during post-cruise processing by including corrections for hole-size changes and temperature variations. A Kalman filtering (Ruckebusch, 1983) is used in the CSU processing at sea to minimize the statistical uncertainties in the logs, which can otherwise create erroneous negative values and anti-correlations (especially between Th and U). An alpha filter has been introduced more recently and is now recommended by Schlumberger for shore-based processing. This filter strongly smooths the raw spectral counts but keeps the total gamma-ray curve unsmoothed before calculating out the Th, U, and K. The outputs of this program are K (wet wt%), U (ppm), and Th (ppm), as well as total gamma-ray and computed gamma-ray (total gamma ray minus U contribution). They are displayed as a function of depth in the log summary figures at the end of the relevant site chapter (this volume).

Step 4: Calculation of Al concentration

The fourth processing routine (PREACT) calculates the concentration of Al in the formation using recorded gamma-ray data from four energy windows on the AACT (Fig. 10). During this step, corrections are made for natural radioactivity, borehole-fluid neutron-capture cross section, formation neutron-capture cross section, formation slowing-down length, and borehole size.

Porosity and density logs are needed as inputs into this routine to convert the wet-weight percentages of K and Al curves to dry weight percentages. To derive the best porosity log, shipboard core porosity measurements were compared with porosity logs calculated from the resistivity (using the relationship of Archie, 1942) and bulk density logs, and taken from the neutron porosity tool. The best correlation with core was found with the density derived porosity and this was used in the PREACT routine.

A correction is also made for Si interference with Al; the ^{252}Cf source activates the Si, producing the aluminum isotope, ^{28}Al, (Hertzog et al., 1989). The program uses the Si yield from the GST to determine the Si background correction. The program outputs dry-weight percentages of Al and K which are combined in the next processing step with the GST-derived elemental yields in the oxide closure model.

Step 5: Normalization of elemental yields from the GST to calculate the elemental weight fractions

Relative concentrations of the GST-derived elemental yields can be determined by dividing each elemental yield by a relative spectral sensitivity factor (S_i). This factor is principally related to the thermal neutron-capture cross sections and also to its gamma-ray production and detection probability of each element (Hertzog et al., 1989). The relative elemental concentrations are related to the desired absolute concentrations by a depth-dependent normalization factor (F), as defined by the relationship:

$$Wt_i = FY_i / S_i, \quad (1)$$

where Wt_i = absolute elemental concentration, and Y_i = relative elemental yield.

The normalization factor is calculated on the basis that the sum of all the elemental weight fractions is unity (100%). The closure model handles the absence of carbon and oxygen, which are not measured by this tool string, with the approximation that each of the measurable elements combines with a known oxide or carbonate. The dry weight percent of Al and K are normalized with the reconstructed elemental yields to determine the normalization factor at each depth interval from the following equation:

$$F(\Sigma_i X_i Y_i / S_i) + X_k Wt_k + X_{Al} Wt_{Al} = 100, \quad (2)$$

where

X_i = oxide factor; atomic weight of the associated oxide or carbonate of element i ÷ atomic weight of element i,
X_k = oxide factor; atomic weight K_2O ÷ atomic weight of K,
Wt_k = dry weight % of K as determined from the NGT,
X_{Al} = oxide factor; atomic weight of Al_2O_3 ÷ atomic weight of Al, and
Wt_{Al} = dry weight % of Al, as determined from the AACT.

The value, X_i, accounts for the C and O associated with each element. Table 6 lists the oxide factors used in this calculation for Hole 984B.

Step 6: Calculation of oxide percentages

This routine converts the elemental weight percentages into oxide percentages by multiplying each by its associated oxide factor, as shown in Table 6. The results are displayed as a function of depth in the log summary figures at the end of the relevant site chapter (this volume). The results are compared to the calcium carbonate measurements performed on board for Hole 984B.

Step 7: Calculation of error logs

The statistical uncertainty of each element is calculated for each of the elements measured with the GST and NGT (Grau et al., 1990; Schweitzer et al., 1988; Bristow et al., 1994). This error is strongly related to the normalization factor, which is calculated at each depth level (Equation 2). Both normalization factor and statistical uncertainties are displayed as a function of depth in the log summary figures at the end of the relevant site chapter in this volume. A lower normalization factor represents better counting statistics and therefore higher quality data.

Table 6. Oxide factors used in normalizing elements to 100% and converting elements to oxides.

Element	Oxide/ carbonate	Conversion factor
Si	SiO_2	2.139
Ca	$CaCO_3$	2.497
Fe	FeO*	1.358
K	K_2O	1.205
Ti	TiO_2	1.668
Al	Al_2O_3	1.889

REFERENCES

Archie, G.E., 1942. The electrical resistivity log as an aid in determining some reservoir characteristics. *Trans. Am. Inst. Min. Metall. Pet. Eng.*, 146:54–62.

ASTM, 1980. Standard method for laboratory determination of water (moisture) content of soil, rock and soil-aggregate mixtures. In *Annual Book of ASTM Standards:* Philadelphia (Am. Soc. Testing and Mater.).

————, 1987. Standard test method for laboratory miniature vane shear test for saturated fine-grained clayey soil. In *Annual Book of ASTM Standards* (Vol. 04.08): Philadelphia (Am. Soc. Testing and Mater.).

Baldauf, J.G., 1984. Cenozoic diatom biostratigraphy and paleoceanography of the Rockall Plateau region, North Atlantic, Deep Sea Drilling Project Leg 81. *In* Roberts, D.G., Schnitker, D., et al., *Init. Repts. DSDP,* 81: Washington (U.S. Govt. Printing Office), 439–478.

————, 1987. Diatom biostratigraphy of the middle- and high-latitude North Atlantic Ocean, Deep Sea Drilling Project Leg 94. *In* Ruddiman, W.F., Kidd, R.B., Thomas, E., et al., *Init. Repts. DSDP,* 94 (Pt. 2): Washington (U.S. Govt. Printing Office), 729–762.

Barron, J.A., 1985. Late Eocene to Holocene diatom biostratigraphy of the equatorial Pacific Ocean, Deep Sea Drilling Project Leg 85. *In* Mayer, L., Theyer, F., Thomas, E., et al., *Init. Repts. DSDP,* 85: Washington (U.S. Govt. Printing Office), 413–456.

————, 1992. Neogene diatom datum levels in the equatorial and North Pacific. *In* Saito, T., and Ishizaki, K. (Eds.), *The Centenary of Japanese Micropaleontology:* Tokyo (Terra Scientific), 413–425.

Barron, J.A., and Gladenkov, A.Y., 1995. Early Miocene to Pleistocene diatom stratigraphy of Leg 145. *In* Rea, D.K., Basov, I.A., Scholl, D.W., and Allan, J.F. (Eds.), *Proc. ODP, Sci. Results,* 145: College Station, TX (Ocean Drilling Program), 3–19.

Berggren, W.A., 1972. Cenozoic biostratigraphy and paleobiogeography of the North Atlantic. *In* Laughton, A.S., Berggren, W.A., et al., *Init. Repts. DSDP,* 12: Washington (U.S. Govt. Printing Office), 965–1002.

Berggren, W.A., Aubry, M.P., and Hamilton, N., 1983. Neogene magnetostratigraphy of Deep Sea Drilling Project Site 516 (Rio Grande Rise, South Atlantic). *In* Barker, P.F., Carlson, R.L., Johnson, D.A., et al., *Init. Repts. DSDP,* 72: Washington (U.S. Govt. Printing Office), 675–713.

Berggren, W.A., Hilgen, F.J., Langereis, C.G., Kent, D.V., Obradovich, J.D., Raffi, I., Raymo, M.E., and Shackleton, N.J., 1995. Late Neogene chronology: new perspectives in high-resolution stratigraphy. *Geol. Soc. Am. Bull.,* 107:1272–1287.

Berggren, W.A., Kent, D.V., Flynn, J.J., and Van Couvering, J.A., 1985. Cenozoic geochronology. *Geol. Soc. Am. Bull.,* 96:1407–1418.

Bjørklund, K.R., 1976. Radiolaria from the Norwegian Sea, Leg 38 of the Deep Sea Drilling Project. *In* Talwani, M., Udintsev, G., et al., *Init. Repts. DSDP,* 38: Washington (U.S. Govt. Printing Office), 1101–1168.

Blow, W.H., 1969. Late middle Eocene to Recent planktonic foraminiferal biostratigraphy. *In* Brönnimann, P., and Renz, H.H. (Eds.), *Proc. First Int. Conf. Planktonic Microfossils, Geneva, 1967:* Leiden (E.J. Brill), 1:199–422.

————, 1979. *The Cainozoic Globigerinida:* Leiden (E.J. Brill).

Bodén, P., 1992. Quantitative biostratigraphy of Neogene diatoms from the Norwegian Sea, North Atlantic and North Pacific. *Stockholm Contrib. Geol.,* 42:124–120.

Bordovskiy, O.K., 1965. Accumulation and transformation of organic substances in marine sediment, 2. Sources of organic matter in marine basins. *Mar. Geol.,* 3:5–31.

Borehole Research Group, 1994. *Wireline Logging Services Guide:* Palisades, NY (Lamont-Doherty Earth Observatory, Columbia Univ.).

Boyce, R.E., 1976. Definitions and laboratory techniques of compressional sound velocity parameters and wet-water content, wet-bulk density, and porosity parameters by gravimetric and gamma-ray attenuation techniques. *In* Schlanger, S.O., Jackson, E.D., et al., *Init. Repts. DSDP,* 33: Washington (U.S. Govt. Printing Office), 931–958.

Bristow, J.F., Lofts, J.C., Harvey, P.K., and Lovell, M.A., 1994. Reservoir characterisation using nuclear geochemical logging. *Trans. 16th Eur. Form. Eval. Symp.,* Aberdeen.

Bukry, D., 1979. Coccolith and silicoflagellate stratigraphy, northern Mid-Atlantic Ridge and Reykjanes Ridge, Deep Sea Drilling Project Leg 49. *In* Luyendyk, B.P., Cann, J.R., et al., *Init. Repts. DSDP,* 49: Washington (U.S. Govt. Printing Office), 551–581.

Cande, S.C., and Kent, D.V., 1992. A new geomagnetic polarity time scale for the Late Cretaceous and Cenozoic. *J. Geophys. Res.,* 97:13917–13951.

————, 1995. Revised calibration of the geomagnetic polarity timescale for the Late Cretaceous and Cenozoic. *J. Geophys. Res.,* 100:6093–6095.

Curry, W.B., Shackleton, N.J., Richter, C., et al., 1995. *Proc. ODP, Init. Repts.,* 154: College Station, TX (Ocean Drilling Program).

Dewan, J.T., 1983. *Essentials of Modern Open-Hole Log Interpretation:* Tulsa (PennWell).

Dzinoridze, R.N., Jousé, A.P., Koroleva-Golikova, G.S., Kozlova, G.E., Nagaeva, G.S., Petrushevskaya, M.G., and Strelnikova, N.I., 1978. Diatom and radiolarian Cenozoic stratigraphy, Norwegian Basin; DSDP Leg 38. *In* Talwani, M., Udintsev, G., et al., *Init. Repts. DSDP,* 38, 39, 40, 41 (Suppl.): Washington (U.S. Govt. Printing Office), 289–427.

Ellis, D.V., 1987. *Well Logging For Earth Scientists:* Amsterdam (Elsevier).

Emeis, K.-C., and Kvenvolden, K.A., 1986. Shipboard organic geochemistry on *JOIDES Resolution. ODP Tech. Note,* 7.

Emerson, S., and Hedges, J.I., 1988. Processes controlling the organic carbon content of open ocean sediments. *Paleoceanography,* 3:621–634.

Farrell, J.W., and Janecek, T.R., 1991. Late Neogene paleoceanography and paleoclimatology of the northeast Indian Ocean (Site 758). *In* Weissel, J., Peirce, J., Taylor, E., Alt, J., et al., *Proc. ODP, Sci. Results,* 121: College Station, TX (Ocean Drilling Program), 297–355.

Fisher, A., and Becker, K., 1993. A guide to ODP tools for downhole measurements. *ODP Tech. Note,* 10.

Gieskes, J.M., Gamo, T., and Brumsack, H., 1991. Chemical methods for interstitial water analysis aboard *JOIDES Resolution. ODP Tech. Note,* 15.

Goll, R.M., and Bjørklund, K.R., 1989. A new radiolarian biostratigraphy for the Neogene of the Norwegian Sea: ODP Leg 104. *In* Eldholm, O., Thiede, J., Taylor, E., et al., *Proc. ODP, Sci. Results,* 104: College Station, TX (Ocean Drilling Program), 697–737.

Grau, J.A., and Schweitzer, J.S., 1989. Elemental concentrations from thermal neutron capture gamma-ray spectra in geological formations. *Nucl. Geophys.,* 3:1–9.

Grau J.A., Schweitzer, J.S., and Hertzog, R.C., 1990. Statistical uncertainties of elemental concentrations extracted from neutron-induced gamma-ray measurements. *IEEE Trans. Nucl. Sci.,* 37:2175–2178.

Hagelberg, T., Shackleton, N., Pisias, N., and Shipboard Scientific Party, 1992. Development of composite depth sections for Sites 844 through 854. *In* Mayer, L., Pisias, N., Janecek, T., et al., *Proc. ODP, Init. Repts.,* 138 (Pt. 1): College Station, TX (Ocean Drilling Program), 79–85.

Hagelberg, T.K., Pisias, N.G., Shackleton, N.J., Mix, A.C., and Harris, S., 1995. Refinement of a high-resolution, continuous sedimentary section for studying equatorial Pacific Ocean paleoceanography, Leg 138. *In* Pisias, N.G., Mayer, L.A., Janecek, T.R., Palmer-Julson, A., and van Andel, T.H. (Eds.), *Proc. ODP, Sci Results,* 138: College Station, TX (Ocean Drilling Program), 31–46.

Hertzog, R.C., Colson, J.L., Seeman, B., O'Brien, M.S., Scott, H.D., McKeon, D.C., Wraight, P.D., Grau, J.A., Ellis, D.V., Schweitzer, J.S., and Herron, M.M., 1989. Geochemical logging with spectrometry tools. *SPE Form. Eval.,* 4:153–162.

Hilgen, F.J., 1991a. Astronomical calibration of Gauss to Matuyama sapropels in the Mediterranean and implication for the geomagnetic polarity time scale. *Earth Planet. Sci. Lett.,* 104:226–244.

————, 1991b. Extension of the astronomically calibrated (polarity) time scale to the Miocene/Pliocene boundary. *Earth Planet. Sci. Lett.,* 107:349–368.

Hooper, P.W.P., and Weaver, P.P.E., 1987. Late Neogene species of the genus *Neogloboquadrina* Bandy, Frerichs and Vincent in the North Atlantic: a biostratigraphic, palaeoceanographic and phylogenetic review. *In* Hart, M.B. (Ed.), *Micropalaeontology of Carbonate Environments:* Chichester (Ellis Horwood), 21–43.

Kaminski, M.A., Gradstein, F.M., Goll, R.M., and Greig, D., 1990. Biostratigraphy and paleoecology of deep-water agglutinated foraminifera at ODP Site 643, Norwegian-Greenland Sea. *In* Hemleben, C., Kaminski, M.A., Kuhnt, W., and Scott, D. (Eds.), *Paleoecology, Biostratigraphy, Paleoceanography and Taxonomy of Agglutinated Foraminifera.* NATO ASI Ser. C, 237:345–386.

Kennett, D.M., and Kennett, J.P., 1991. *Bolboforma* Daniels and Spiegler, from Eocene and lower Oligocene sediments, Maud Rise, Antarctica. *In* Barker, P.F., Kennett, J.P., et al, *Proc. ODP, Sci. Results,* 113: College Station, TX (Ocean Drilling Program), 667–673.

Kvenvolden, K.A., and McDonald, T.J., 1986. Organic geochemistry on the *JOIDES Resolution*—an assay. *ODP Tech. Note,* 6.

Lazarus, D., and Pallant, A., 1989. Oligocene and Neogene radiolarians from the Labrador Sea, ODP Leg 105. *In* Srivastava, S.P., Arthur, M.A., Clement, B., et al., *Proc. ODP, Sci. Results,* 105: College Station, TX (Ocean Drilling Program), 349–380.

Lock, G.A., and Hoyer, W.A., 1971. Natural gamma-ray spectral logging. *The Log Analyst,* 12:3–9.

Locker, S., in press. Paleogene silicoflagellates from the Fram Strait and the East Greenland Margin: biostratigraphic and paleoceanographic results of Leg 151. *In* Thiede, J., Myhre, A.M., Firth, J.V., Johnson, G.L., and Ruddiman, W.F. (Eds.), *Proc. ODP, Sci. Results,* 151: College Station, TX (Ocean Drilling Program).

Locker, S., and Martini, E., 1989. Cenozoic silicoflagellates, ebridians, and actiniscidians from the Vøring Plateau (ODP Leg 104). *In* Eldholm, O., Thiede, J., Taylor, E., et al., *Proc. ODP, Sci. Results,* 104: College Station, TX (Ocean Drilling Program), 543–585.

Manheim, F.T., and Sayles, F.L., 1974. Composition and origin of interstitial waters of marine sediments, based on deep sea drill cores. *In* Goldberg, E.D. (Ed.), *The Sea* (Vol. 5): *Marine Chemistry: The Sedimentary Cycle:* New York (Wiley), 527–568.

Manum, S.B., Boulter, M.C., Gunnarsdottir, H., Rangnes, K., and Scholze, A., 1989. Eocene to Miocene palynology of the Norwegian Sea (ODP Leg 104). *In* Eldholm, O., Thiede, J., Taylor, E., et al., *Proc. ODP, Sci. Results,* 104: College Station, TX (Ocean Drilling Program), 611–662.

Martini, E., 1979. Calcareous nannoplankton and silicoflagellate biostratigraphy at Reykjanes Ridge, northeastern North Atlantic (DSDP Leg 49, Sites 407 and 409). *In* Luyendyk, B.P., Cann, J.R., et al., *Init. Repts. DSDP,* 49: Washington (U.S. Govt. Printing Office), 533–549.

Martini, E., and Müller, C., 1976. Eocene to Pleistocene silicoflagellates from the Norwegian-Greenland Sea (DSDP Leg 38). *In* Talwani, M., Udintsev, G., et al., *Init. Repts. DSDP,* 38: Washington (U.S. Govt. Printing Office), 857–895.

Mazzullo, J.M., Meyer, A., and Kidd, R.B., 1988. New sediment classification scheme for the Ocean Drilling Program. *In* Mazzullo, J., and Graham, A.G. (Eds.), *Handbook for Shipboard Sedimentologists.* ODP Tech. Note, 8:45–67.

Mix, A.C., Rugh, W., Pisias, N.G., Veirs, S., Leg 138 Shipboard Sedimentologists (Hagelberg, T., Hovan, S., Kemp, A., Leinen, M., Levitan, M., Ravelo, C.), and Leg 138 Scientific Party, 1992. Color reflectance spectroscopy: a tool for rapid characterization of deep-sea sediments. *In* Mayer, L., Pisias, N., Janecek, T., et al., *Proc. ODP, Init. Repts.,* 138 (Pt. 1): College Station, TX (Ocean Drilling Program), 67–77.

Müller, C., and Spiegler, D., 1993. Revision of late/middle Miocene boundary on the Voering Plateau (ODP Leg 104). *Newsl. Stratigr.,* 28:171–178.

Myhre, A.M., Thiede, J., Firth, J.V., et al., 1995. *Proc. ODP, Init. Repts.,* 151: College Station, TX (Ocean Drilling Program).

Nigrini, C., and Lombari, G., 1984. *A Guide to Miocene Radiolaria.* Spec. Publ. Cushman Found. Foraminiferal Res., 22.

Nigrini, C., and Moore, T.C., 1979. *A Guide to Modern Radiolaria.* Spec. Publ. Cushman Found. Foraminiferal Res., 16.

Nigrini, C., and Sanfilippo, A., 1992. Cenozoic radiolarian stratigraphy for low and middle latitudes. Catalogue compiled for ODP. [Unpublished]

Okada, H., and Bukry, D., 1980. Supplementary modification and introduction of code numbers to the low-latitude coccolith biostratigraphic zonation (Bukry, 1973; 1975). *Mar. Micropaleontol.,* 5:321–325.

Pages, G., Etchopar, A., Moulin, P., and Pocachard, J., 1993. Harnessing paleomagnetics for logging. *Oilfield Review,* 10.

Perch-Nielsen, K., 1978. Eocene to Pliocene archaeomonads, ebridians, and endoskeletal dinoflagellates from the Norwegian Sea, DSDP Leg 38. *In*

Talwani, M., Udintsev, G., et al., *Init. Repts. DSDP,* 38 (Suppl.): Washington (U.S. Govt. Printing Office), 147–175.

————, 1985. Silicoflagellates. *In* Bolli, H.M., Saunders, J.B., and Perch-Nielsen, K. (Eds.), *Plankton Stratigraphy:* Cambridge (Cambridge Univ. Press), 811–846.

Posamentier, H.W., Jervey, M.T., and Vail, P.R., 1988. Eustatic controls on clastic deposition, I: conceptual framework. *In* Wilgus, C.K., Hastings, B.S., Ross, C.A., Posamentier, H.W., Van Wagoner, J., and Kendall, C.G.St.C. (Eds.), *Sea-Level Changes: An Integrated Approach.* Spec. Publ.—Soc. Econ. Paleontol. Mineral., 42:109–124.

Pozzi, J.-P., Martin, J.P., Pocachard, J., Feinberg, H., and Galdeano, A., 1988. In situ magnetostratigraphy: interpretation of magnetic logging in sediments. *Earth Planet. Sci. Lett.,* 88:357–373.

Pratson, E.L., Broglia, C., and Jarrard, R., 1993. Data report: geochemical well logs through Cenozoic and Quaternary sediments from Sites 815, 817, 820, 822, and 823. *In* McKenzie, J.A., Davies, P.J., Palmer-Julson, A., et al., *Proc. ODP, Sci. Results,* 133: College Station, TX (Ocean Drilling Program), 795–817.

Qvale, G., and Spiegler, D., 1989. The stratigraphic significance of *Bolboforma* (algae, Chrysophyta) in Leg 104 samples from the Vøring Plateau. *In* Eldholm, O., Thiede, J., Taylor, E., et al., *Proc. ODP, Sci. Results,* 104: College Station, TX (Ocean Drilling Program), 487–495.

Raymo, M.E., Ruddiman, W.F., Backman, J., Clement, B.M., and Martinson, D.G., 1989. Late Pliocene variation in Northern Hemisphere ice sheets and North Atlantic deep water circulation. *Paleoceanography,* 4:413–446.

Ruckebusch, G., 1983. A Kalman filtering approach to natural gamma ray spectroscopy in well logging. *IEEE Trans. Autom. Control,* AC-28:372–380.

Ruddiman, W.F., Cameron, D., and Clement, B.M., 1987. Sediment disturbance and correlation of offset holes drilled with the hydraulic piston corer: Leg 94. *In* Ruddiman, W.F., Kidd, R.B., Thomas, E., et al., *Init. Repts. DSDP,* 94 (Pt. 2): Washington (U.S. Govt. Printing Office), 615–634.

Schlumberger, 1989. *Log Interpretation Principles/Applications:* Houston, TX (Schlumberger Educ. Services).

————, 1994. *Geological High-Resolution Magnetic Tool (GHMT) Interpretation Method:* Paris, France (Schlumberger Riboud Product Center).

Schrader, H.-J., and Fenner, J., 1976. Norwegian Sea Cenozoic diatom biostratigraphy and taxonomy. *In* Talwani, M., Udintsev, G., et al., *Init. Repts. DSDP,* 38: Washington (U.S. Govt. Printing Office), 921–1099.

Schweitzer, J.S., Grau, J.A., and Hertzog, R.C., 1988. Precision and accuracy of short-lived activation measurements for in situ geological analyses. *J. Trace Microprobe Techniques,* 6:437–451.

Scott, H.D., and Smith, M.P., 1973. The aluminum activation log. *The Log Analyst,* 14:3–12.

Shackleton, N.J., Berger, A., and Peltier, W.A., 1990. An alternative astronomical calibration of the lower Pleistocene timescale based on ODP Site 677. *Trans. R. Soc. Edinburgh: Earth Sci.,* 81:251–261.

Skempton, A.W., and Bishop, A.W., 1950. The measurement of the shear strength of soils. *Geotechnique,* 2:90–108.

Spiegler, D., 1991. Occurrence of *Bolboforma* (Algae, Chrysophyta) in the subantarctic (Atlantic) Paleogene. *In* Ciesielski, P.F., Kristoffersen, Y., et al., *Proc. ODP, Sci. Results,* 114: College Station, TX (Ocean Drilling Program), 325–334.

Spiegler, D., and von Daniels, C.H., 1991. A stratigraphic and taxonomic atlas of *Bolboforma* (Protophytes, Incertae sedis, Tertiary). *J. Foraminiferal Res.,* 21:126–158.

Spiegler, D., and Jansen, E., 1989. Planktonic foraminifer biostratigraphy of Norwegian Sea sediments: ODP Leg 104. *In* Eldholm, O., Thiede, J., Taylor, E., et al., *Proc. ODP, Sci. Results,* 104: College Station, TX (Ocean Drilling Program), 681–696.

Spiegler, D., and Müller, C., 1992. Correlation of *Bolboforma* zonation and nannoplankton stratigraphy in the Neogene of the North Atlantic: DSDP Sites 12-116, 49-408, 81-555 and 94-608. *Mar. Micropaleontol.,* 20:45–58.

Takahashi, K., 1991. *Radiolaria: Flux, Ecology, and Taxonomy in the Pacific and Atlantic.* Ocean Biocoenosis Ser., 3: Woods Hole, MA (WHOI).

Thomas, E., 1987. Late Oligocene to Recent foraminifers from Deep Sea Drilling Project Sites 608 and 610, northeastern North Atlantic. *In* Ruddiman, W.F., Kidd, R.B., Thomas, E., et al., *Init. Repts. DSDP,* 94: Washington (U.S. Govt. Printing Office), 997–1031.

Timur, A., and Toksöz, M.N., 1985. Downhole geophysical logging. *Annu. Rev. Earth Planet. Sci.,* 13:315–344.

Vail, P.R., Mitchum, R.M., Jr., Todd, R.G., Widmier, J.M., Thompson, S., III, Sangree, J.B., Bubb, J.N., and Hatlelid, W.G., 1977. Seismic stratigraphy and global changes in sea level. *In* Payton, C.E. (Ed.), *Seismic Stratigraphy: Applications to Hydrocarbon Exploration.* AAPG Mem., 26:49–221.

Weaver, P.P.E., and Clement, B.M., 1986. Synchroneity of Pliocene planktonic foraminiferal datums in the North Atlantic. *Mar. Micropaleontol.,* 10:295–307.

————, 1987. Magnetobiostratigraphy of planktonic foraminiferal datums, DSDP Leg 94, North Atlantic. *In* Ruddiman, W.F., Kidd, R.B., Thomas, E., et al., *Init. Repts. DSDP,* 94: Washington (U.S. Govt. Printing Office), 815–829.

Wentworth, C.K., 1922. A scale of grade and class terms of clastic sediments. *J. Geol.,* 30:377–392.

Wessel, P., and Smith, W.H.F., 1991. Free software helps map and display data. *Eos,* 72:441, 445–446.

Westberg-Smith, M.J., and Riedel, W.R., 1984. Radiolarians from the western margin of the Rockall Plateau: Deep Sea Drilling Project Leg 81. *In* Roberts, D.G., Schnitker, D., et al., *Init. Repts. DSDP,* 81: Washington (U.S. Govt. Printing Office), 479–501.

Williams, G.L., and Bujak, J.P., 1985. Mesozoic and Cenozoic dinoflagellates. *In* Bolli, H.M, Saunders, J.B., and Perch-Nielsen, K. (Eds.), *Plankton Stratigraphy:* Cambridge (Cambridge Univ. Press), 847–964.

Ms 162IR-102